Direct numerical simulation of turbulent heat transfer in an axially rotating pipe flow

Reynolds shear stress and scalar flux budgets

Shin-ichi Satake
Department of Applied Electronics, Tokyo University of Science, Yamazaki, Noda, Chiba, Japan
Tomoaki Kunugi
Department of Nuclear Engineering, Kyoto University, Yoshida, Sakyou, Kyoto, Japan

Keywords *Numerical simulation, Turbulent flow, Rotating flows*

Abstract *A direct numerical simulation with turbulent transport of a scalar quantity has been carried out to grasp and understand a laminarization phenomena caused by a pipe rotation. In this study, the Reynolds number, which is based on a bulk velocity and a pipe diameter, was set to be constant;* $Re_b = 5283$*, and the rotating ratios of a wall velocity to a bulk velocity were set to be 0.5, 1.0, 2.0 and 3.0. A uniform heat-flux was applied to the wall as a thermal boundary condition. Prandtl number of the working fluid was assumed to be 0.71. The number of computational grids used in this study was* $256 \times 128 \times 128$ *in the* z-, r- *and* ϕ- *directions, respectively. The turbulent quantities such as the mean flow, temperature fluctuations, turbulent stresses and pressure distribution and the turbulent statistics were obtained. Moreover, the Reynolds stress and the scalar flux budgets were also obtained for each rotating ratio. The turbulent drag decreases with the rotating ratio increase. The reason of this drag reduction can be considered that the additional rotational production terms appear in the azimuthal turbulence component. The contributions of convection and production terms to the radial scalar flux budget and also to the balance with temperature-pressure gradient term are significant. The dissipation and viscous diffusion terms are negligible in higher rotating ratio.*

I. Introduction

The utilization of heat transfer with turbulent swirling flow has often appeared in many mechanical and chemical engineering fields; inlet part of a fluid machinery, enhancement of mixing and chemical reaction in combustion chamber, etc. Therefore, many experimental and numerical studies for the effect of swirling flow on heat, mass and momentum transports have been carried out in the world.

As for the velocity field of swirling flows, many experimental studies (Murakami and Kikuyama, 1980; Kikuyama *et al.*, 1983; Nishibori *et al.*, 1987) have been carried out during past decade. Several numerical studies by

International Journal of Numerical Methods for Heat & Fluid Flow, Vol. 12 No. 8, 2002, pp. 958-1008.

DOI 10.1108/09615530210448723

ensemble average turbulence models regarding an axially rotating pipe flow have been carried out; Hirai *et al.* (1988) used a Reynolds shear stress model and Kawamura and Mishima (1992) used a two-equation model of turbulence. These numerical studies predicted the drag reduction and the parabolic velocity profile in circumferential velocity and were in good agreement with the experimental data.

Recently, the turbulent drag reduction has been predicted by a large eddy simulation (Eggels, 1994) and the direct numerical simulation (DNS) Orlandi and Fatica (1997). Orlandi (1997) shows, the turbulent quantities and the probability density function of helicity. Orlandi and Ebstein (2000) investigate turbulent kinetic energy and Reynolds shear stresses budget. However, scalar flux budget have not been presented. On the other hand, the only two experiments regarding the heat transfer in an axially rotating pipe flow have been carried out by Cannon and Kays (1969) and Reich and Beer (1989). While the numerical study regarding both velocity and heat transfer for rotating pipe flows has been reported by Satake and Kunugi (1999). They investigate turbulent kinetic energy, Reynolds shear stress and scalar flux budgets in the range of lower rotating ratio ($N = 0.25$, 0.3 and 0.35). In spite of low rotating ratio, the budgets of additional Reynolds stress $u_r u_\phi$, $u_z u_\phi$ owing to pipe rotation affect the mechanism of momentum and heat transfer.

The objectives of this study are to present turbulent kinetic energy, Reynolds shear stress and scalar flux budget using DNS and to elucidate the mechanism of the momentum and heat transfer due to the pipe rotation through these equations in the range of higher rotating ratio (N = 0.5, 1.0, 2.0 and 3.0).

II. Numerical procedure

The DNS code (Satake and Kunugi, 1999) with cylindrical coordinates can numerically solve the momentum and continuity equations. A second-order finite volume discretization scheme is applied to the spatial derivatives on a staggered mesh system. In order to avoid a singularity at the center axis of the pipe center, the incompressible Navier-Stokes equation can be rewritten with a radial flux formulation. The radial momentum equation in conservative form can be discretized as the same manner as Verzicco and Orlandi (1996). The incompressible Navier-Stokes and continuity equations described in cylindrical coordinate are integrated in time using the fractional-step method by Dukowics and Divinsky (1992). A modified third-order Runge-Kutta scheme (Spalart *et al.*, 1991) is applied to the nonlinear terms treated explicitly and the second-order Crank-Nicholson scheme is used for other terms implicitly. In our previous study regarding turbulent pipe flow (Satake and Kunugi, 1998 a, b), this DNS code has been shown in good agreement with the previous DNS results obtained by Eggels *et al.* (1994).

The energy equation is described as:

$$\frac{\partial T}{\partial t}+\frac{\partial u_z T}{\partial z}+\frac{1}{r}\frac{\partial r u_r T}{\partial r}+\frac{1}{r}\frac{\partial u_\phi T}{\partial \phi} = \frac{1}{\mathrm{Re}_\tau \mathrm{Pr}}\left[\frac{\partial^2 T}{\partial z^2}+\frac{1}{r}\frac{\partial}{\partial r}\left(r\frac{\partial T}{\partial r}\right)+\frac{1}{r^2}\frac{\partial^2 T}{\partial \phi^2}\right] \tag{1}$$

The constant heat flux on the wall is defined by

$$q_0 = -\lambda \left.\frac{\mathrm{d}T}{\mathrm{d}r}\right|_R \tag{2}$$

The computational domain with the wall heated by above heat flux q_0 are shown in Figure 1. To impose the constant heat flux on the wall, the nondimensional temperature is defined as:

$$\theta^+(z,r,\phi,t) = \left\{\langle T_w\rangle_{z,\phi} - T(z,r,\phi,t)\right\}/T_\tau \tag{3}$$

where T_w and T_τ are the wall temperature and friction temperature, respectively, and $\langle\,\rangle_{z,\phi}$ express the average with respect to z, ϕ. This method adopted channel flow (Kasagi *et al.*, 1992) and annulus flow (Kawamura *et al.*, 1992). The gradient of the bulk temperature $T_m = \langle T\rangle_{r,z,\phi}$ expressed by

$$\frac{\mathrm{d}T_m}{\mathrm{d}z} = \frac{2q_0}{\rho c_p U_b R} \tag{4}$$

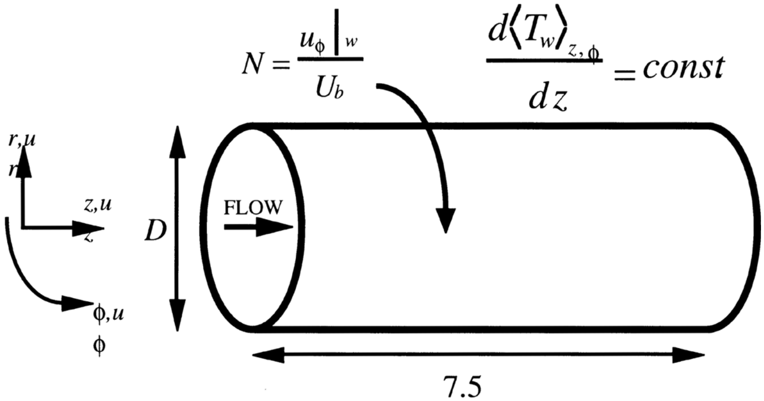

Figure 1.
Computational domain

where U_b is the mean bulk temperature. The nondimensional form of equation (1) is derived by

$$\frac{\partial \theta^+}{\partial t}+\frac{\partial u_z \theta^+}{\partial z}+\frac{1}{r}\frac{\partial r u_r \theta^+}{\partial r}+\frac{1}{r}\frac{\partial u_\phi \theta^+}{\partial \phi}$$
$$=\frac{1}{Pe_\tau}\left[\frac{\partial^2 \theta^+}{\partial z^2}+\frac{1}{r}\frac{\partial}{\partial r}\left(r\frac{\partial \theta^+}{\partial r}\right)+\frac{1}{r^2}\frac{\partial^2 \theta^+}{\partial \phi^2}\right]+2\frac{u_z}{U_b} \quad (5)$$

The boundary condition at the wall is also expressed as

$$\theta^+(z,R,\phi,t)=0 \quad (6)$$

The equation (5) also can be discretized as the finite volume method and are integrated in time using a modified third-order Runge-Kutta scheme (Spalart *et al.*, 1991) is applied to the nonlinear terms treated explicitly and the second-order Crank-Nicholson scheme is used for other terms implicitly.

III. Computational condition

The computational domain of the fully developed turbulent pipe flow is shown in Figure 1. The number of grid points is $256 \times 128 \times 128$ in the z-, r- and ϕ -directions, respectively. The Reynolds number, which is based on bulk velocity and pipe diameter D, is set to be constant; $\mathrm{Re_b} = 5283$, and the rotating ratios N of a wall velocity $u_\phi|_\mathrm{w}$ to a bulk velocity U_b were set to be 0.5, 1.0, 2.0 and 3.0. A uniform heat-flux was applied to the wall as a thermal boundary condition. Prandtl number of the working fluid was set to be 0.71. Further details of the velocity boundary condition for pipe geometry DNS can be found in Satake and Kunugi (1998a). The result was in good agreement with Eggel's (1994) DNS data. As an initial condition, instantaneous velocity and scalar fields at fully developed state were taken from the data of Satake and Kunugi (1998a). After the velocity and thermal fields were judged to be fully developed, the time integration of the repetition for obtaining the turbulent statistics as an ensemble average was about 3,240 ν/u_τ^2 (180,000 steps).

IV. Results and discussion

Figure 2(a) and (b) show the axial mean velocity and temperature profiles normalized by bulk velocity and temperature difference ($T_\mathrm{w} - \mathrm{T_c}$), respectively. T_w and T_c are the wall and center temperatures, respectively. In velocity profiles, excellent agreement between the present and Orlandi and Fatica's (1997) results is obtained at every rotating ratio. However, both these profiles are fairly in good agreement with the experimental result of Reich and Beer (1989). In accordance with Orlandi and Fatica (1997), the discrepancy can be the influence of the entrance condition in the experimental measurement by Reich

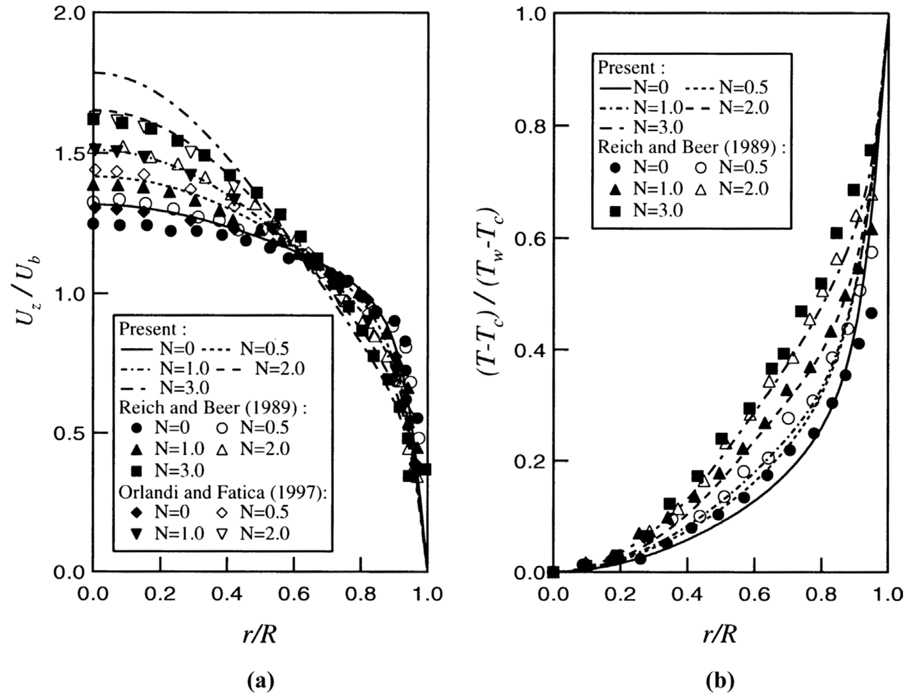

Figure 2.
(a) The axial mean velocity, (b) temperature profiles

and Beer (1989). The results of the present DNS and Orlandi and Fatica's (1997) one are fully developed turbulent flow. The temperature profiles in Figure 2(b) show a similar trend.

Table I shows the friction coefficients and Nusselt number for every rotating number. The reduction rate λ/λ_0 of the wall friction $\lambda = 8(u_\tau/U_b)^2$ in the present simulation is also in good agreement with the results of Orlandi and Fatica's (1997) DNS.

The present results of the streamwise velocity profiles normalized by friction velocity u_τ are compared with the existing DNS results for four rotating ratios investigated as shown in Figure 3.

Table I.
The friction coefficients and Nusselt number for every rotating number

N	λ/λ_0(SK)	λ/λ_0(OF)	Nu/Nu_0(SK)
0.0	1.0	1.0	1.0
0.5	0.8658	0.8386	0.9311
1.0	0.8533	0.8290	0.92278
2.0	0.8304	0.8247	0.8858
3.0	0.7874	–	0.8132

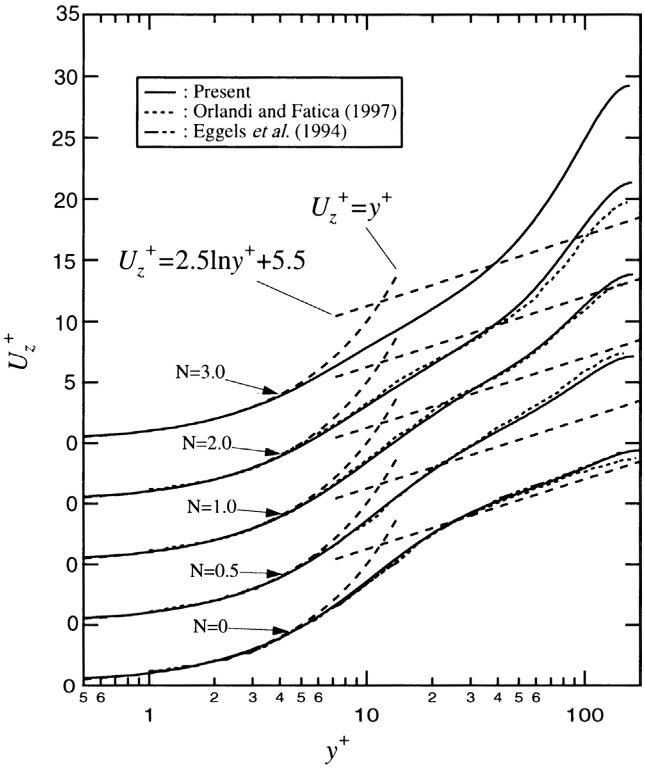

Figure 3.
The present results of the streamwise velocity profiles normalized by friction velocity

At $N = 0.0$, the present profile is exactly in agreement with that of Eggles *et al.* (1994). The agreement of other turbulent quantities are described in Satake and Kunugi (1998a, b). The agreement between the present and Orlandi and Fatica's (1997) results is very good at $N = 0.5$, 1.0 and 2.0. The present profiles show that the log-low region disappears with increasing rotating ratio. The same tendency was observed by Orlandi and Fatica's (1997) results.

Figure 4 shows the mean temperature distribution normalized by friction temperature. The distributions of the mean temperature are similar to that of the mean velocity. At lower N, the logarithmic region shifts up, while at higher N, the logarithmic region disappears and the buffer region seems to be enlarged.

The velocity fluctuations normalized by bulk velocity U_b are shown in Figure 5(a)-(c). The results with $N = 0$ and 2 by Orlandi and Fatica (1997) are also plotted in Figure 5(a)-(c) with open symbols. In case of $N = 0.0$ and 2.0, good agreements between the present and Orlandi and Fatica's (1997) velocities are obtained. Isotropy among the turbulence components is pronounced in the near wall region. The streamwise and circumferential components are the most

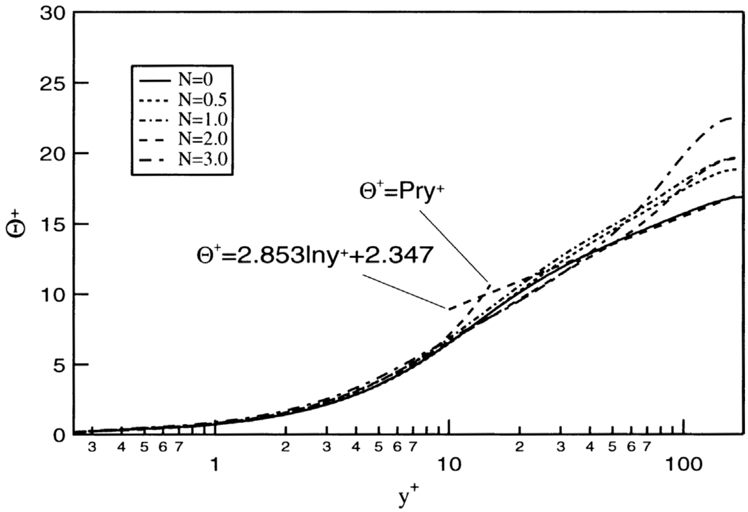

Figure 4.
The temperature distribution normalized by friction temperature

energetic and have the same value at $N = 3.0$, because the latter is produced directly by the mean circumferential velocity.

Figure 6 shows nondimensional temperature fluctuation normalized friction temperature versus the wall coordinate (y^+). The peak point moves slightly towards the center pipe with increase of the rotating ratio. This behavior is similar to velocity fluctuation of streamwise component as shown in Figure 5(a).

Figure 7 shows the total and the Reynolds shear stresses $\overline{u'^+_z u'^+_r}$ normalized by the friction velocity. Almost all cases are in good agreement with Orlandi and Fatica's results (1997). With increase of N, the distribution of $\overline{u'^+_z u'^+_r}$ decrease from the location of the peak to the pipe center.

Figure 8 shows the Reynolds shear stresses $\overline{u'^+_r u'^+_\phi}$ normalized by the friction velocity. This stress is strongly affected by the pipe rotation. At $N = 0.5$, 1.0 and 2.0, the present results show an excellent agreement between the present results and with Orlandi and Fatica's (1997) results. At $N = 3.0$, the Reynolds stress is most enhanced in the whole region.

Figure 9 shows the Reynolds shear stresses $\overline{u'^+_z u'^+_\phi}$ normalized by the friction velocity. Results obtained by Orlandi and Fatica's (1997) show that there are regions of negative correlation. They indicate that the radial oscillation of $\overline{u'^+_z u'^+_\phi}$ at high N is due to the large scale structures in the center of the pipe. The present results also show similar oscillations at higher N. To restrict these oscillations more computational time is required.

Figures 10-12 show scalar fluxes of $\overline{u'^+_z \theta' +}$, $\overline{u'^+_r \theta' +}$ and $\overline{u'^+_\phi \theta'^+}$ normalized by the friction velocity, respectively. At $N = 0.5$ and 1.0, the location of maximum point is the same compared with $N = 0.0$. The peak point decreases at $N = 2.0$, 3.0. This is similar to the distribution of $\overline{u'^+_z u'^+_z}$. According to this

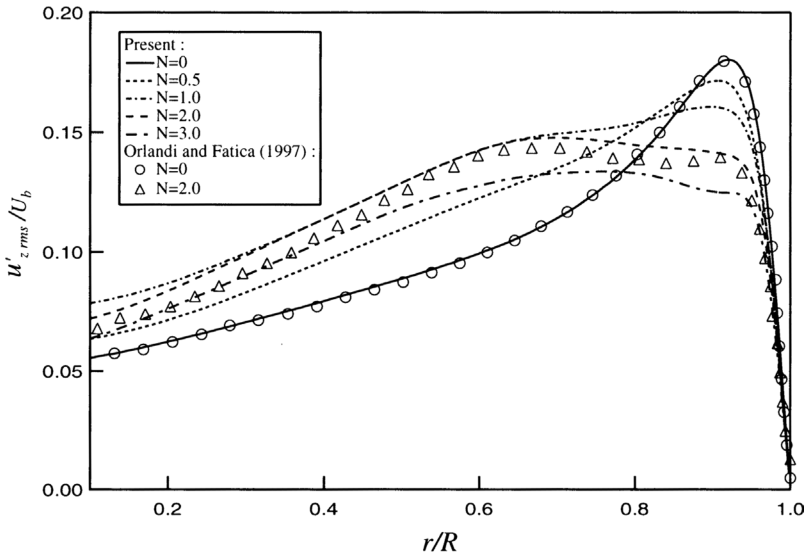

(a)

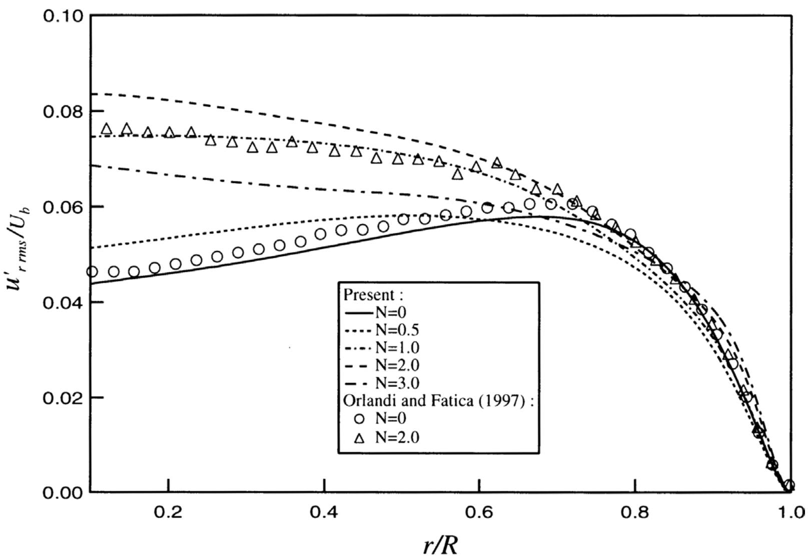

(b)

(*Continued*)

Figure 5.
The velocity fluctuations normalized by bulk velocity U_b, (a) streamwise component, (b) radial component, (c) circumferencial component

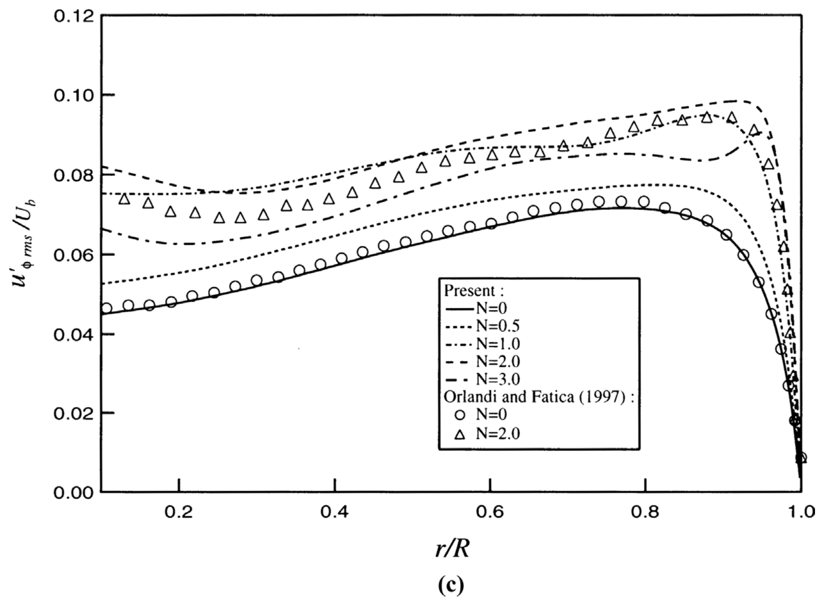

Figure 5.

result, it is evident that u'^{+}_{z} and θ'^{+} are strongly correlated. The distribution of $u'^{+}_{r}\theta'^{+}$ decreases from the location of peak point to the pipe center. It is most pronounced at higher N. At higher N, the radial oscillation takes place at the whole region such as $u'^{+}_{z}u'^{+}_{\phi}$. This shows the strong correlation between u'^{+}_{z} and θ'^{+}.

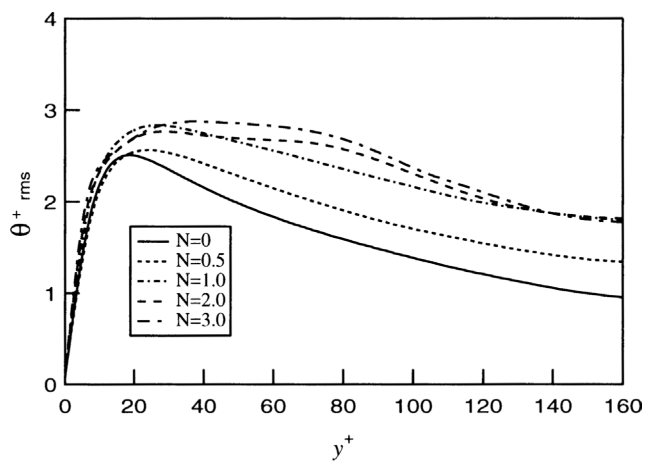

Figure 6.
Temperature fluctuation normalized friction temperature

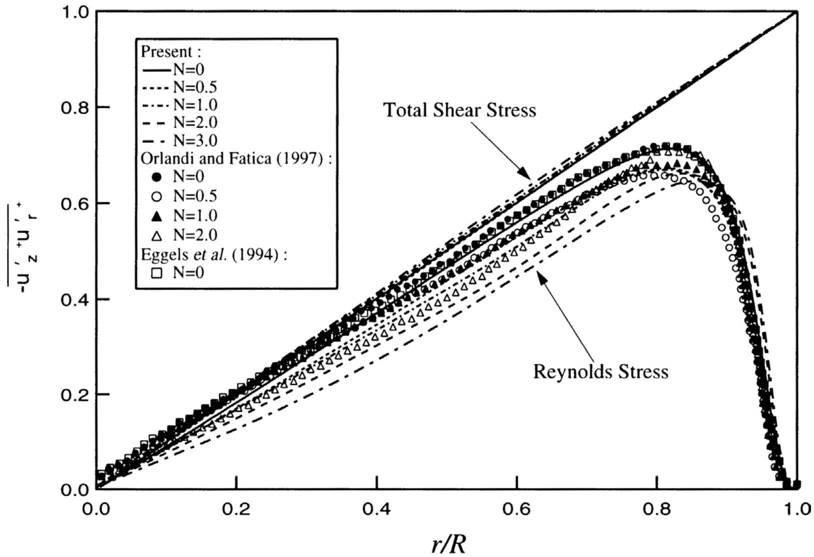

Figure 7. The total and the Reynolds shear stresses normalized by the friction velocity

The fully developed turbulent field in rotating pipe is homogeneous in both the streamwise and circumferential directions, therefore, the budget equation for the turbulent kinetic energy k normalized by the friction velocity can be expressed as:

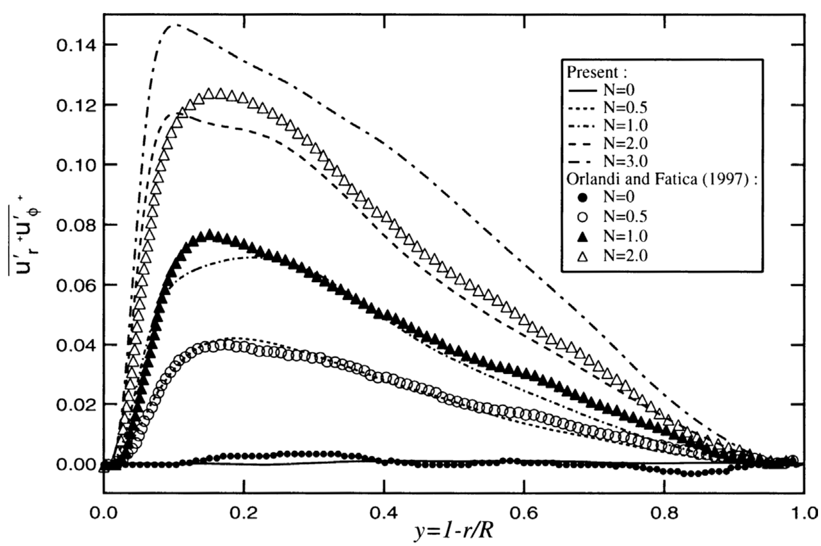

Figure 8. The Reynolds shear stresses $u'^{+}_{r}u'^{+}_{\phi}$ normalized by the friction velocity

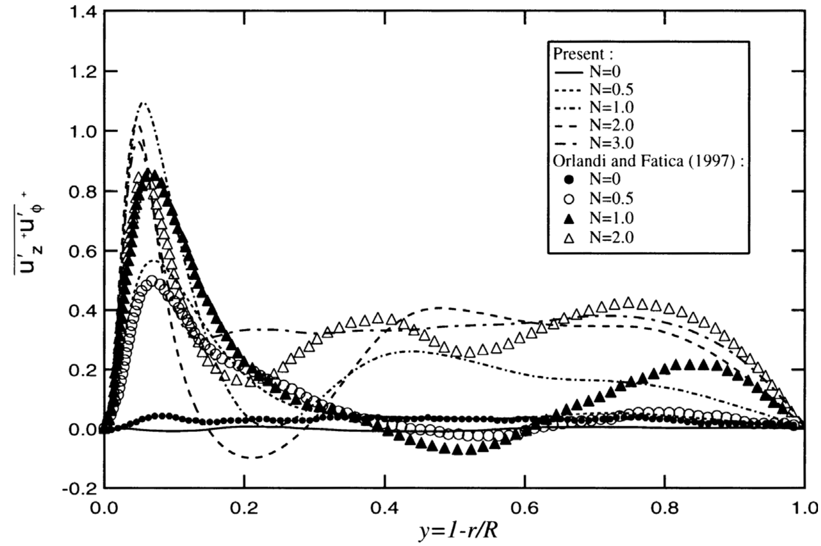

Figure 9.
The Reynolds shear stresses $\overline{u_z'^+ u_\phi'^+}$ normalized by the friction velocity

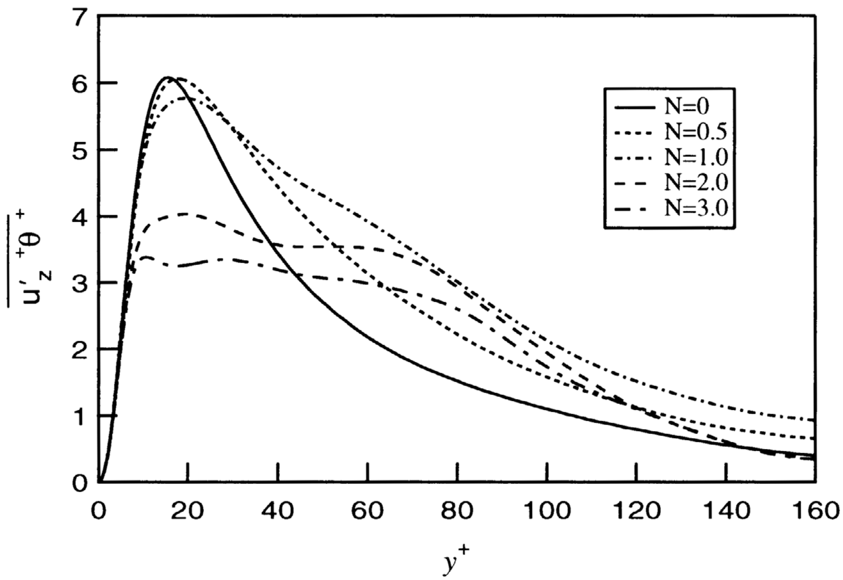

Figure 10.
Scalar flux $\overline{u_z'^+ \theta'^+}$ normalized by the friction velocity

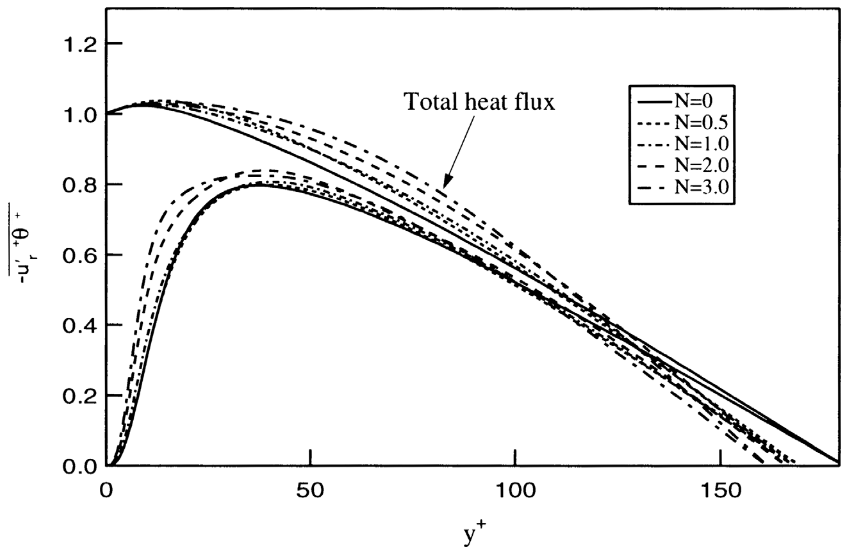

Figure 11.
Scalar flux $\overline{u'^{+}_{r}\theta'+}$ normalized by the friction velocity

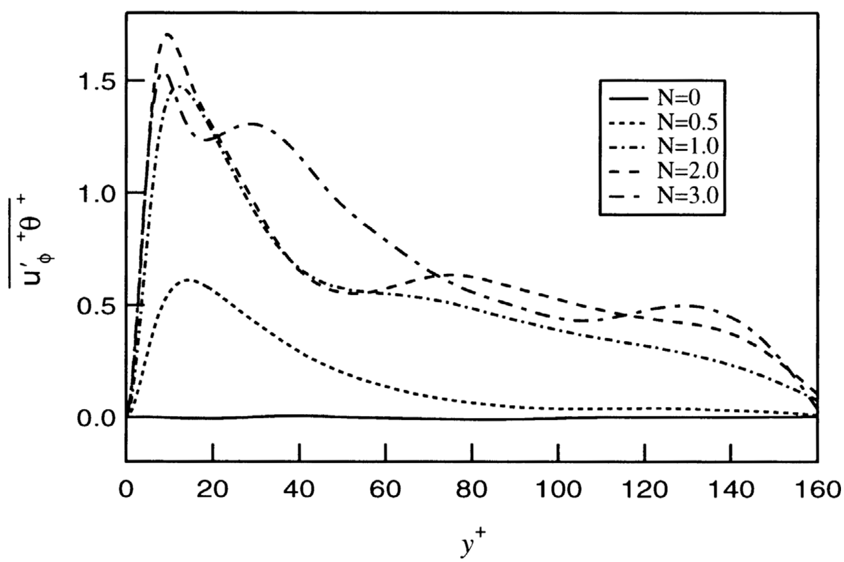

Figure 12.
Scalar flux $\overline{u'^{+}_{\phi}\theta'^{+}}$ normalized by the friction velocity

$$0 = \underbrace{-\frac{1}{r^+}\frac{\partial r^+ \overline{k^+ {u'}_r^+}}{\partial r^+}}_{\text{Turbulent diffusion}} \underbrace{-\overline{{u'}_r^+ {u'}_z^+}\frac{\partial U_z^+}{\partial r^+} + \overline{{u'}_r^+ {u'}_\phi^+}\frac{U_\phi^+}{r^+} - \overline{{u'}_r^+ {u'}_\phi^+}\frac{\partial U_\phi^+}{\partial r^+}}_{\text{Production}}$$

$$\underbrace{-\frac{1}{r^+}\frac{\partial r^+ \overline{p'^+ {u'}_r^+}}{\partial r^+}}_{\text{Pressure diffusion}} \underbrace{+\frac{1}{r^+}\frac{\partial}{\partial r^+}\left(r^+\frac{\partial k^+}{\partial r^+}\right)}_{\text{Viscous diffusion}}$$

$$-\left[+\overline{\left(\frac{\partial {u'}_r^+}{\partial z^+}\right)^2} + \overline{\left(\frac{\partial {u'}_\phi^+}{\partial r^+}\right)^2} + \overline{\left(\frac{1}{r^+}\frac{\partial {u'}_\phi^+}{\partial \phi} + \frac{{u'}_r^+}{r^+}\right)^2} + \overline{\left(\frac{\partial {u'}_\phi^+}{\partial z^+}\right)^2}\right]$$

$$\underbrace{-\left[\overline{\left(\frac{\partial {u'}_z^+}{\partial r^+}\right)^2} + \overline{\left(\frac{1}{r^+}\frac{\partial {u'}_z^+}{\partial \phi}\right)^2} + \overline{\left(\frac{\partial {u'}_z^+}{\partial z^+}\right)^2} + \overline{\left(\frac{\partial {u'}_r^+}{\partial r^+}\right)^2} + \overline{\left(\frac{1}{r^+}\frac{\partial {u'}_r^+}{\partial \phi} - \frac{{u'}_\phi^+}{r^+}\right)^2}\right]}_{\text{Dissipation}} \quad (7)$$

Figure 13(a)-(e) shows each term in equation (7) for each rotating ratios. At the wall, the viscous term balances the dissipation term. The magnitude of these increases with the high rotating ratio increases.

The budget of temperature variance $k_\theta = \frac{1}{2}\bar{\theta}'^2$ is derived as:

$$0 = \underbrace{-\frac{1}{r^+}\frac{\partial r^+ \overline{\theta'^{+^2}/2{u'}_r^+}}{\partial r^+}}_{\text{Turbulent diffusion}} \underbrace{-\overline{{u'}_r^+ \theta'^+}\frac{\partial \Theta}{\partial r^+} + \overline{{u'}_z^+ \theta'^+}\frac{\partial \langle T\rangle^+}{\partial z^+}}_{\text{Production}}$$

$$\underbrace{+\frac{1}{\Pr}\frac{1}{r^+}\frac{\partial}{\partial r^+}\left(r^+\frac{\partial \overline{\theta'^{+^2}/2}}{\partial r^+}\right)}_{\text{Viscous diffusion}} \quad (8)$$

$$\underbrace{-\frac{1}{\Pr}\left\{\overline{\left(\frac{\partial \theta'^+}{\partial z^+}\right)^2} + \overline{\left(\frac{\partial \theta'^+}{\partial r^+}\right)^2} + \frac{1}{r^+}\overline{\left(\frac{\partial \theta'^+}{\partial \phi}\right)^2}\right\}}_{\text{Dissipation}}$$

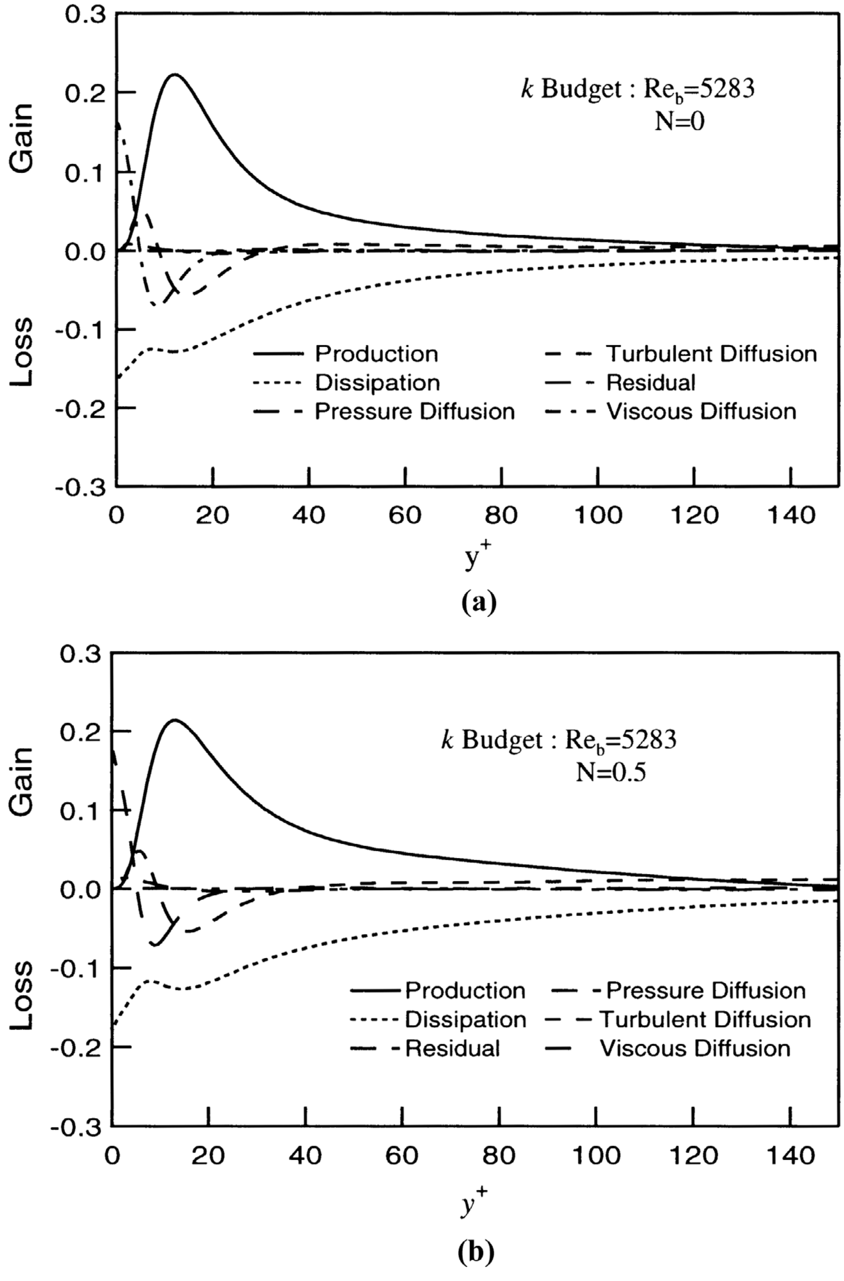

(*Continued*)

Figure 13.
The budget equation for the turbulent kinetic energy k

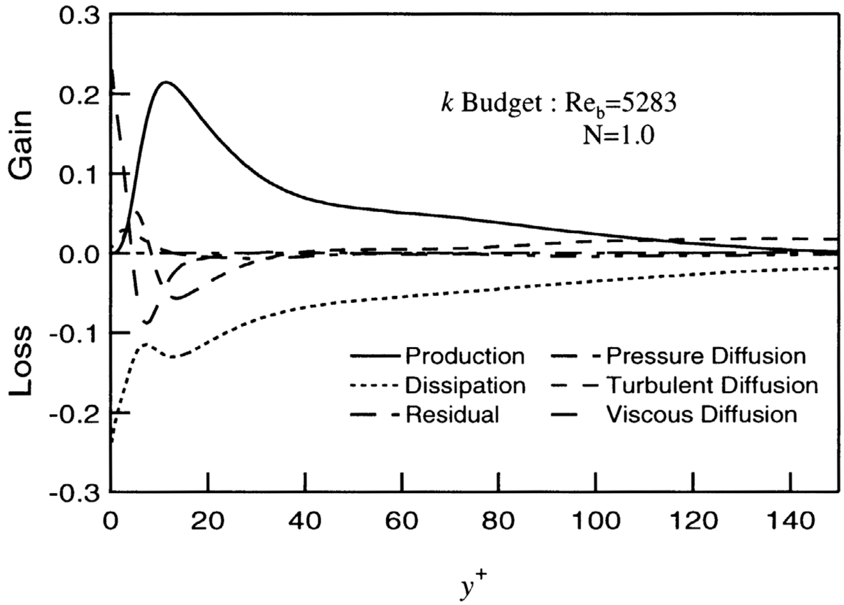

(c)

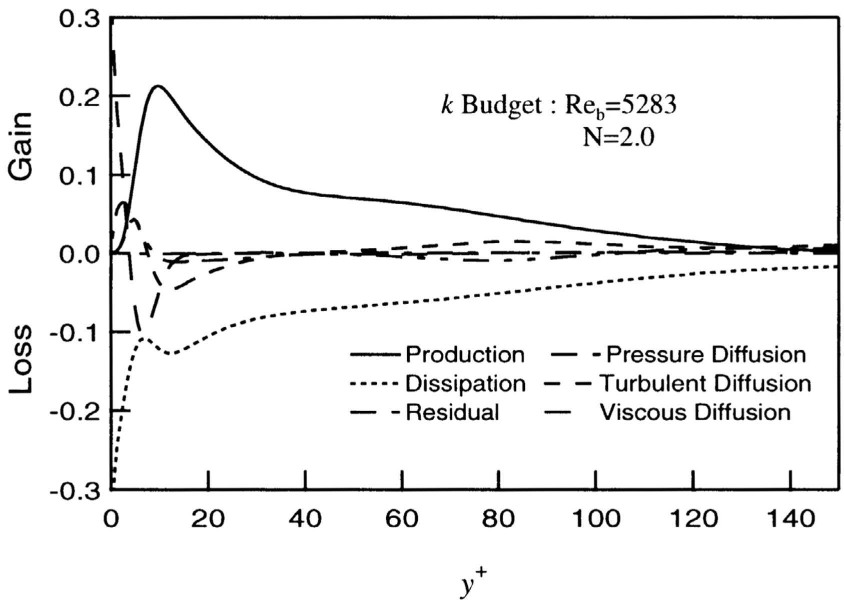

(d)

Figure 13.

(Continued)

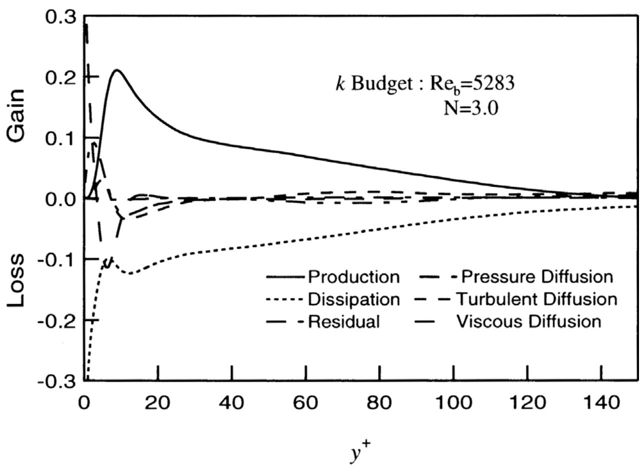

(e)

Figure 13.

Figure 14(a)-(e) shows the temperature variance budget normalized by the friction velocity. The budget of k and k_θ agree well because of the Reynolds analogy. All terms increase with the increase of N.

The budget equations for the $u'^{+}_{z}u'^{+}_{z}$ is rewritten as:

$$0=\underbrace{-\frac{1}{r}\frac{\partial r\overline{u'^{+}_{r}u'^{+}_{z}u'^{+}_{z}}}{\partial r}}_{\text{Turbulent diffusion}}\underbrace{-2\overline{u'^{+}_{r}u'^{+}_{z}}\frac{\partial U_z}{\partial r}}_{\text{Production}}\underbrace{-2\left(\overline{u'^{+}_{z}\frac{\partial p'}{\partial z}}\right)}_{\text{Pressure diffusion}}$$

$$\underbrace{+\frac{1}{r}\frac{\partial}{\partial r}\left(r\frac{\partial\overline{u'^{+}_{z}u'^{+}_{z}}}{\partial r}\right)}_{\text{Viscous diffusion}}\underbrace{-2\left[\overline{\left(\frac{\partial u'^{+}_{z}}{\partial r^{+}}\right)^2}+\overline{\left(\frac{1}{r^{+}}\frac{\partial u'^{+}_{z}}{\partial \phi}\right)^2}+\overline{\left(\frac{\partial u'^{+}_{z}}{\partial z^{+}}\right)^2}\right]}_{\text{Dissipation}} \quad (9)$$

Figure 15(a)-(e)shows the Reynolds shear stress $\overline{u'^{+}_{z}u'^{+}_{z}}$ budget normalized by the friction velocity. The production is a dominant gain term in the whole region. A half of the production is lost by the dissipation, while the other is redistributed to $u'^{+}_{r}u'^{+}_{r}$ and $u'^{+}_{\phi}u'^{+}_{\phi}$ through the pressure strain correlation. The pressure strain terms play a key role to the other normal stress because the effect of rotating on the terms does not appear explicitly in equation (9).

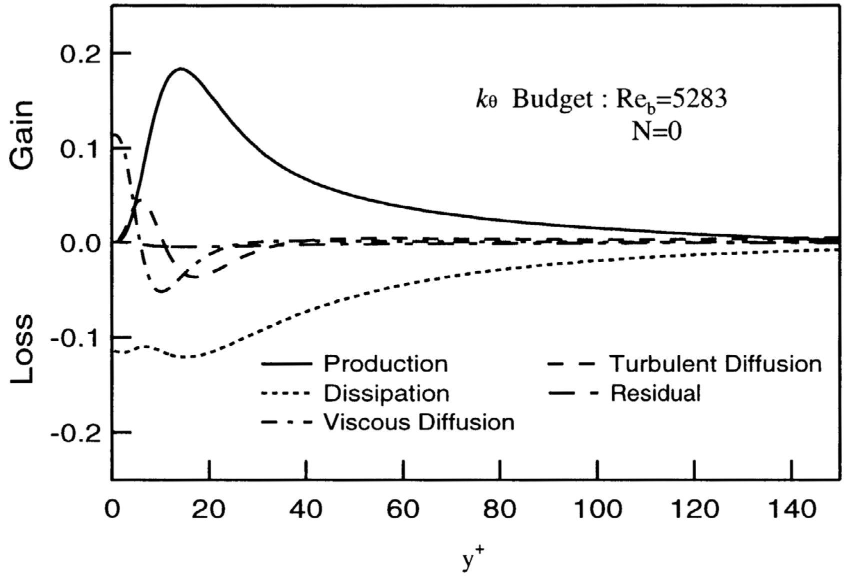

(a)

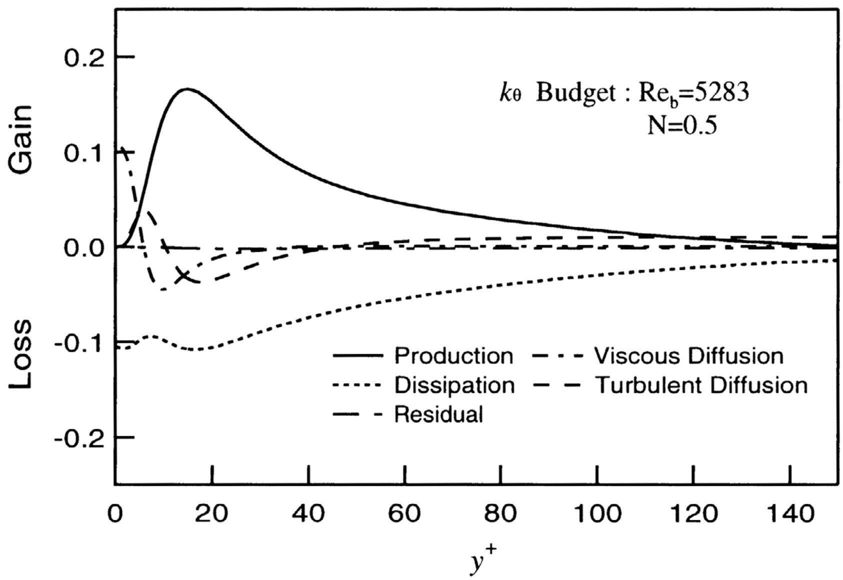

(b)

Figure 14.
The budget equation for the temperature variance k_θ

(Continued)

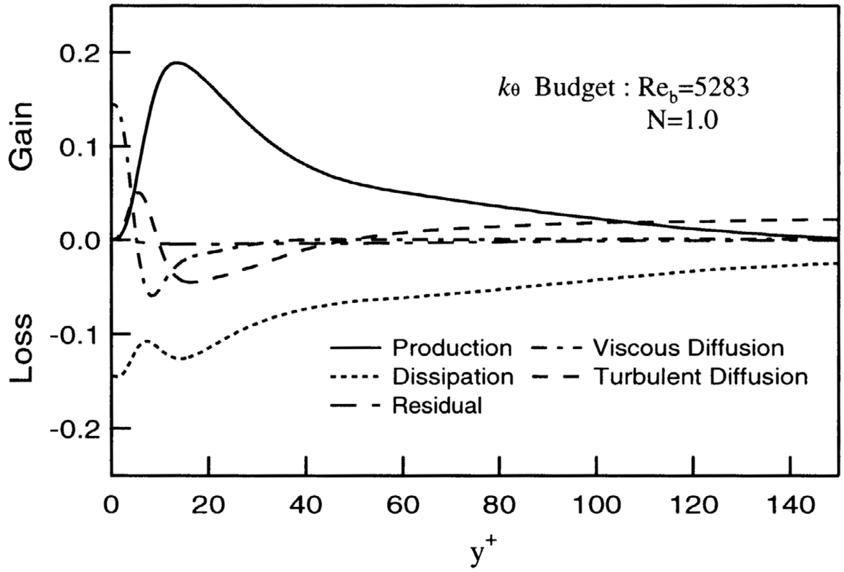

(c)

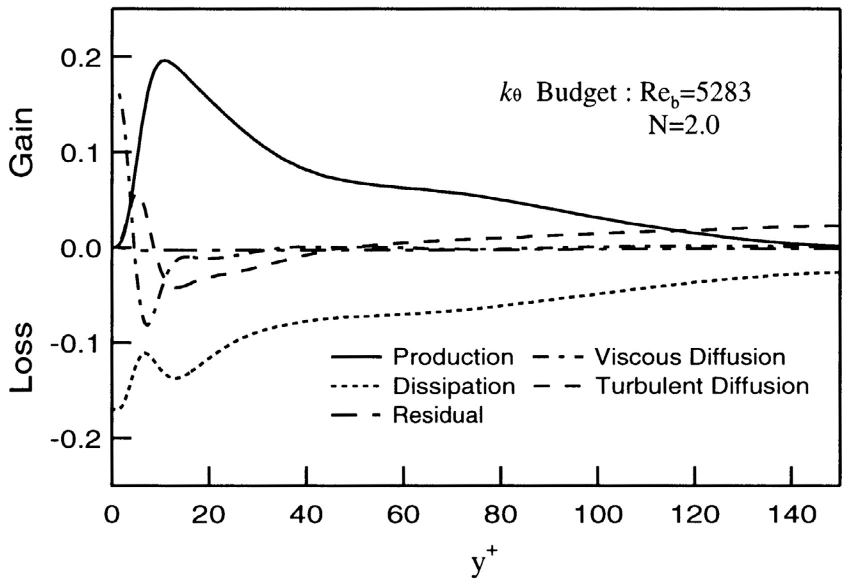

(d)

Figure 14.

(*Continued*)

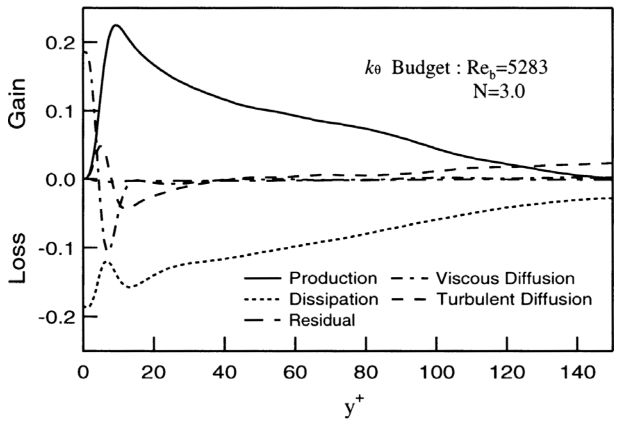

(e)

Figure 14.

The budget equations for the $\overline{u'^+_z u'^+_r}$ is rewritten as:

$$0=\underbrace{-\frac{1}{r^+}\frac{\partial r\overline{u'^+_r u'^+_r u'^+_z}}{\partial r^+}+\frac{\overline{u'^+_z u'^+_\phi u'^+_\phi}}{r^+}}_{\text{Turbulent diffusion}}\underbrace{-\overline{u'^+_r u'_r{}^+}\frac{\partial U^+_z}{\partial r^+}+\overline{u'^+_\phi u'^+_z}\frac{U^+_\phi}{r^+}}_{\text{Production}}$$

$$\underbrace{+\overline{u'^+_\phi u'^+_z}\frac{U^+_\phi}{r^+}}_{\text{Convective transport}}\ \underbrace{-\frac{\overline{u'^+_z\partial p'^+}}{\partial r^+}-\frac{\overline{u'^+_r\partial p'^+}}{\partial z^+}}_{\text{Velocity pressure gradient}}$$

$$\underbrace{+\frac{1}{\mathrm{Re}_\tau}\left[\frac{1}{r^+}\frac{\partial}{\partial r^+}\left(r^+\frac{\partial\overline{u'^+_r u'^+_z}}{\partial r^+}\right)-\frac{\overline{u'^+_r u'^+_z}}{r^{+2}}\right]}_{\text{Viscous diffusion}}$$

$$\underbrace{-\frac{2}{\mathrm{Re}_\tau}\left[\overline{\left(\frac{\partial u'^+_r}{\partial r^+}\right)\left(\frac{\partial u'^+_z}{\partial r^+}\right)}+\overline{\left(\frac{1}{r^+}\frac{\partial u'^+_r}{\partial\phi}-\frac{u'^+_\phi}{r^+}\right)\left(\frac{1}{r^+}\frac{\partial u'^+_z}{\partial\phi}\right)}+\overline{\left(\frac{\partial u'^+_r}{\partial z^+}\right)\left(\frac{\partial u'^+_z}{\partial z^+}\right)}\right]}_{\text{Dissipation}}$$

(10)

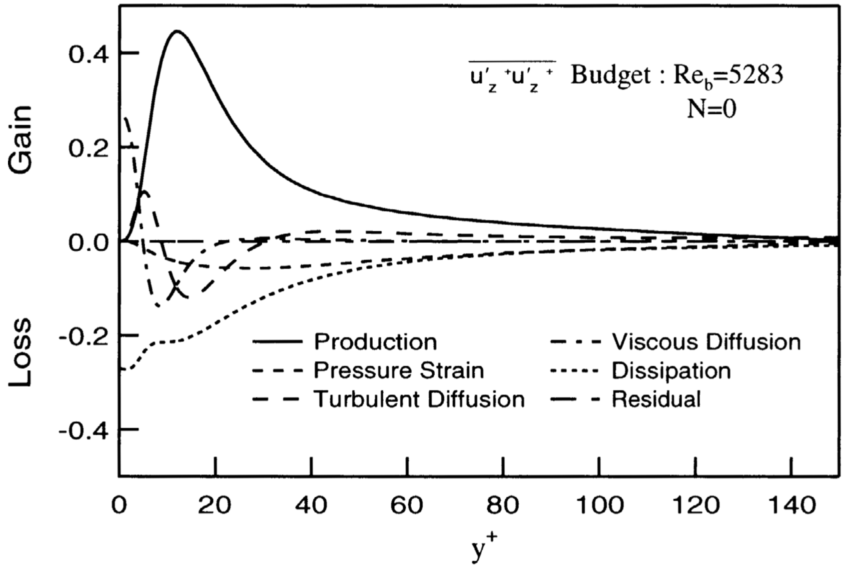

(a)

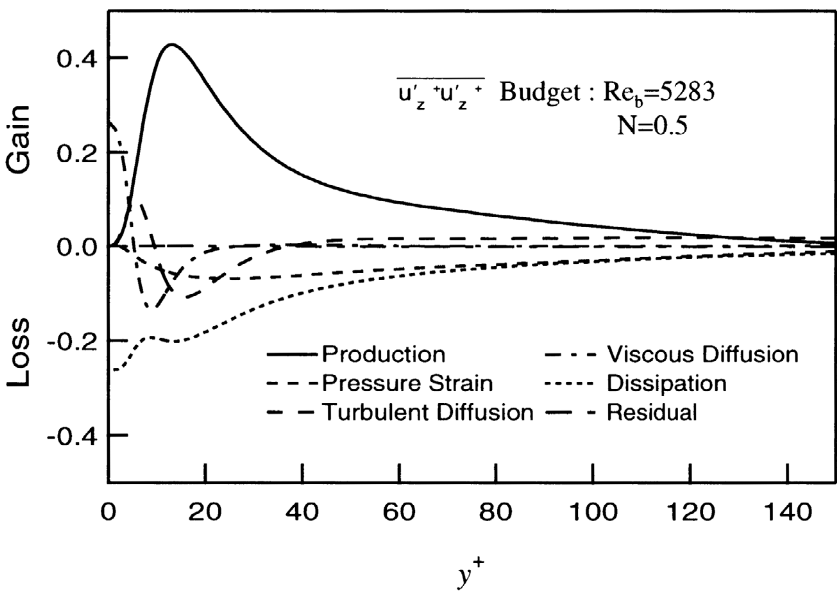

(b)

(*Continued*)

Figure 15.
The Reynolds shear stress $\overline{u'^+_z u'^+_z}$ budget normalized by the friction velocity

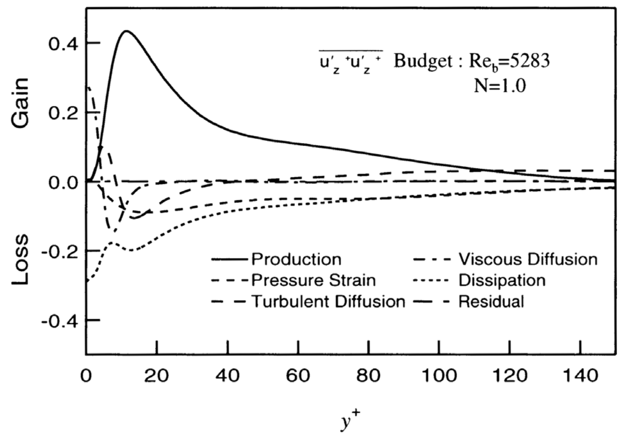

(c)

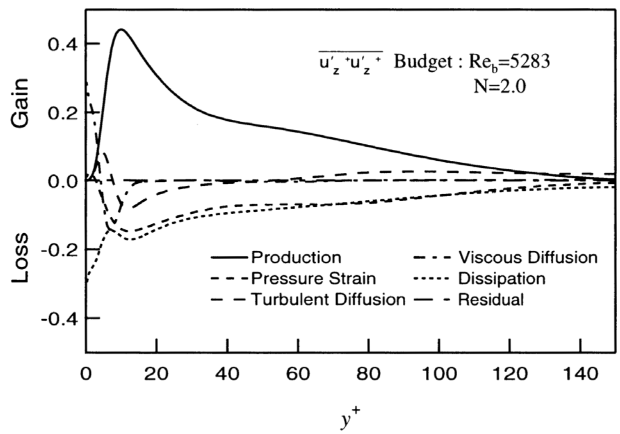

(d)

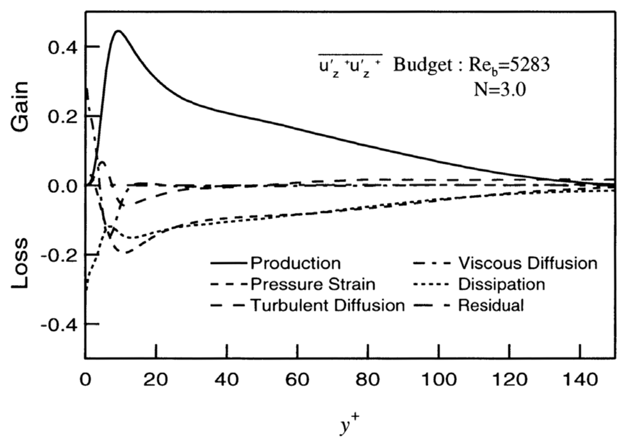

(e)

Figure 15.

Figure 16(a)-(e) shows the Reynolds shear stress $\overline{u'^+_z u'^+_r}$ budget normalized by the friction velocity. The convection, production and the velocity pressure gradient terms are the dominant ones in the whole region. The distribution of three terms in case of $N \geq 1$ shows the concave shape at $y^+ = 30$. This is because mean circumferential velocity U_ϕ increases near wall region. Similar behavior is also shown in the result of Orlandi and Ebstein (2000). The other terms are negligibly small.

The budget equations for the $\overline{u'^+_z u'^+_\phi}$ is rewritten as:

$$0 = -\underbrace{\frac{1}{r^+}\frac{\partial r^+ \overline{u'^+_r u'^+_\phi u'^+_z}}{\partial r^+} - \frac{\overline{u'^+_r u'^+_\phi u'^+_z}}{r^+}}_{\text{Turbulent diffusion}} - \underbrace{\overline{u'^+ r u'^+_z}\frac{\partial U^+_\phi}{\partial r^+} - \overline{u'^+_r u'^+_\phi}\frac{\partial U^+_z}{\partial r^+}}_{\text{Production}}$$

$$- \underbrace{\overline{u'^+_r u'^+_z}\frac{U^+_\phi}{r^+}}_{\text{Convective transport}} - \underbrace{\frac{\overline{u'^+_z \frac{1}{r^+}\partial p'^+}}{\partial \phi} - \frac{\overline{u'^+_\phi \partial p'^+}}{\partial z^+}}_{\text{Velocity pressure gradient}}$$

$$+ \underbrace{\frac{1}{\mathrm{Re}_\tau}\left[\frac{1}{r^+}\frac{\partial}{\partial r^+}\left(r^+ \frac{\partial \overline{u'^+_\phi u'^+_z}}{\partial r^+}\right) - \frac{\overline{u'^+_\phi u'^+_z}}{r^{+2}}\right]}_{\text{Viscous diffusion}}$$

$$- \underbrace{\frac{2}{\mathrm{Re}_\tau}\left[\overline{\left(\frac{\partial u'^+_\phi}{\partial r^+}\right)\left(\frac{\partial u'^+_z}{\partial r^+}\right)} + \overline{\left(\frac{1}{r^+}\frac{\partial u'^+_\phi}{\partial \phi} + \frac{u'^+_r}{r^+}\right)\left(\frac{1}{r^+}\frac{\partial u'^+_z}{\partial \phi}\right)} + \overline{\left(\frac{\partial u'^+_\phi}{\partial z^+}\right)\left(\frac{\partial u'^+_z}{\partial z^+}\right)}\right]}_{\text{Dissipation}} \tag{11}$$

Figure 17(a)-(e) shows the Reynolds shear stress $\overline{u'^+_z u'^+_\phi}$ budget normalized by the friction velocity. For all cases, the viscous term balances the dissipation term at the wall. The dominant term is the velocity-pressure-gradient (VPG) term in the whole region, which balance the sum of the convection and the production terms.

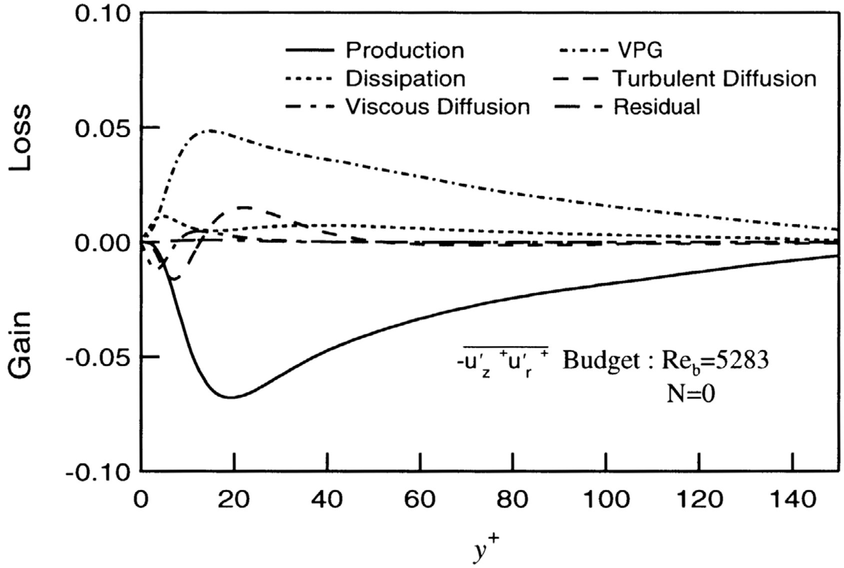

(a)

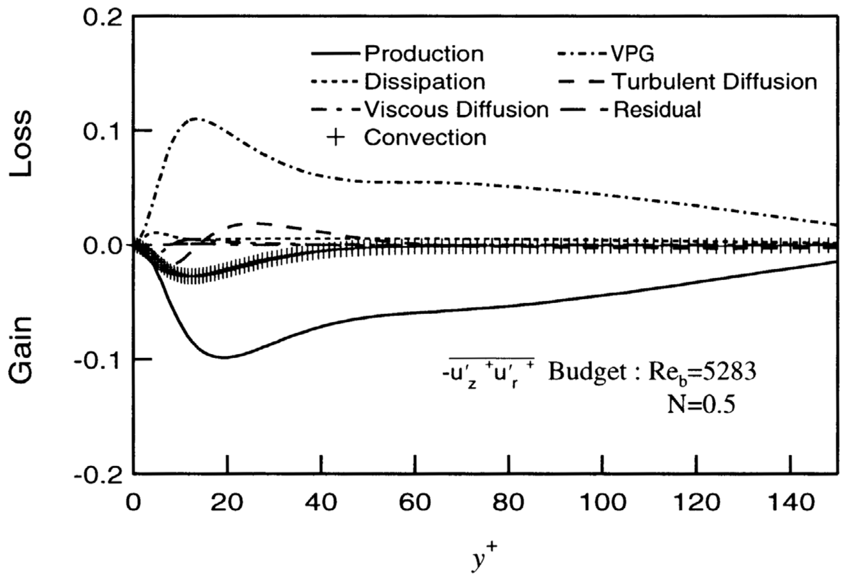

(b)

Figure 16.
The Reynolds shear stress $\overline{u_z'^+ u_r'^+}$ budget normalized by the friction velocity

(Continued)

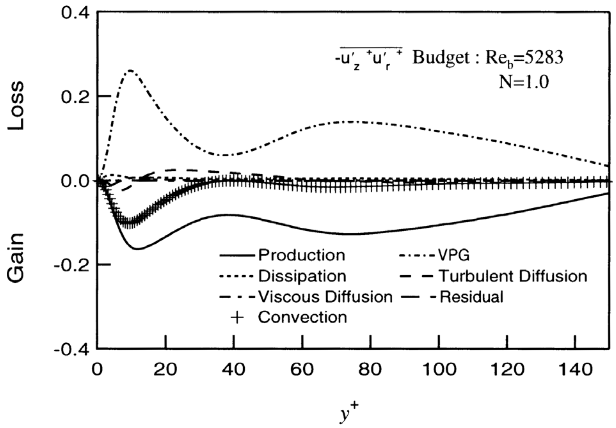

(c)

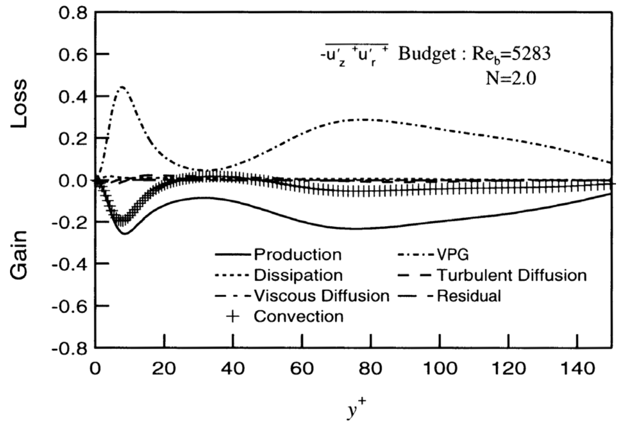

(d)

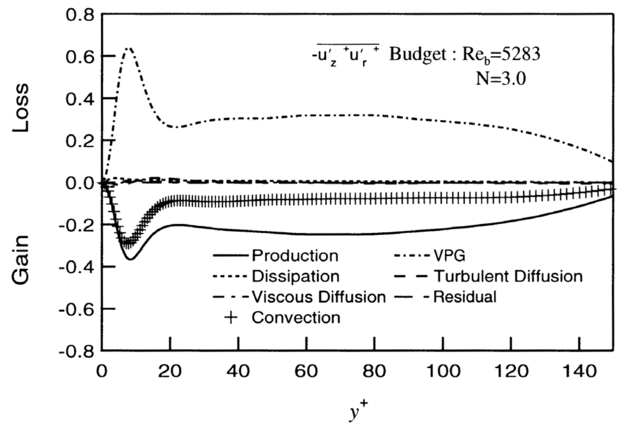

(e)

Figure 16.

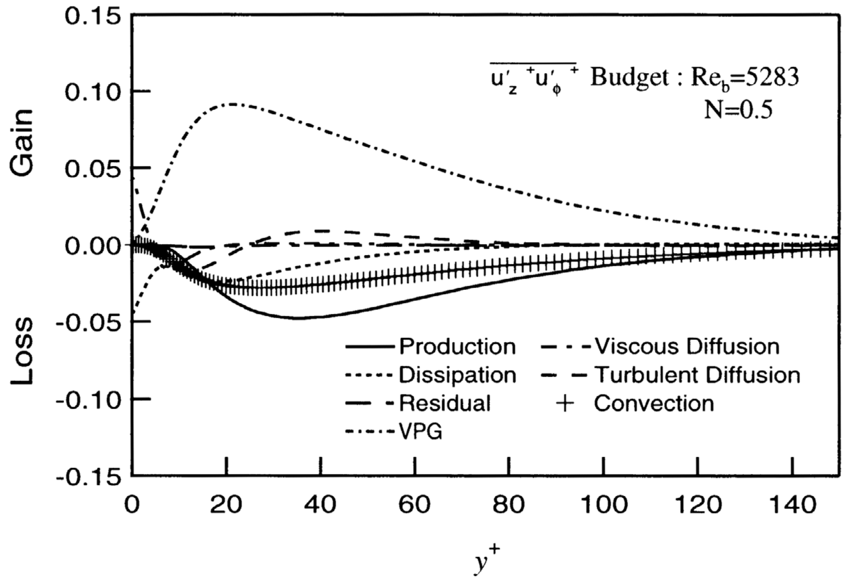

(a)

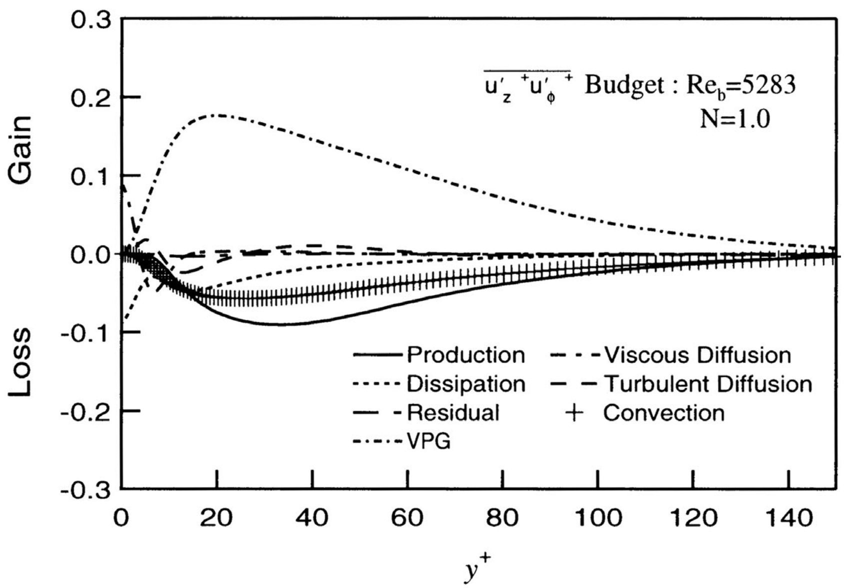

(b)

Figure 17.
The Reynolds shear stress $\overline{u'^+_z u'^+_\phi}$ budget normalized by the friction velocity

(Continued)

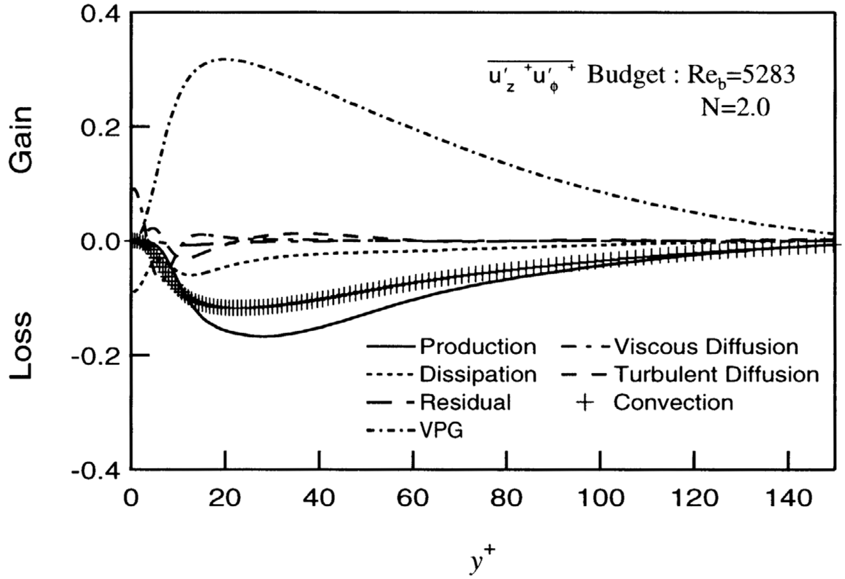
$\overline{u'_z{}^+ u'_\phi{}^+}$ Budget : Re_b=5283
N=2.0
Gain
Loss
Production
Dissipation
Residual
VPG
Viscous Diffusion
Turbulent Diffusion
Convection
0.4
0.2
0.0
-0.2
-0.4
0
20
40
60
80
100
120
140
y^+

(c)

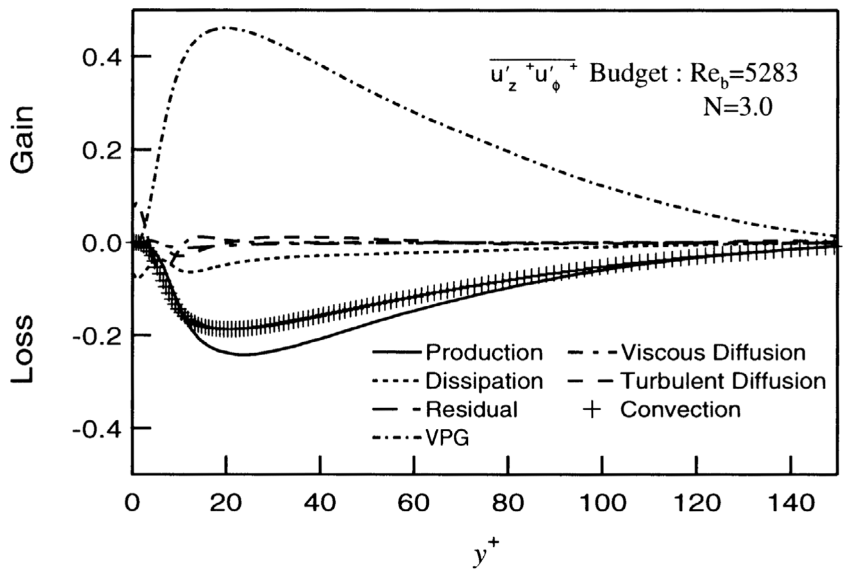
$\overline{u'_z{}^+ u'_\phi{}^+}$ Budget : Re_b=5283
N=3.0
Gain
Loss
Production
Dissipation
Residual
VPG
Viscous Diffusion
Turbulent Diffusion
Convection
0.4
0.2
0.0
-0.2
-0.4
0
20
40
60
80
100
120
140
y^+

(d)

Figure 17.

The following budget equations for the $\overline{u'^+_r u'^+_\phi}$ is rewritten as:

$$0 = -\underbrace{\frac{1}{r^+}\frac{\partial r^+\overline{u'^+_r u'^+_r u'^+_\phi}}{\partial r^+} + \frac{\overline{u'^+_\phi u'^+_\phi u'^+_\phi}}{r^+} - \frac{\overline{u'^+_r u'^+_r u'^+_\phi}}{r^+}}_{\text{Turbulent diffusion}}$$

$$-\underbrace{\overline{u'^+_r u'^+_r}\frac{\partial U^+_\phi}{\partial r^+} + \overline{u'^+_\phi u'^+_\phi}\frac{U^+_\phi}{r^+}}_{\text{Production}} - \underbrace{\overline{u'^+_r u'^+_r}\frac{U^+_\phi}{r^+} + \overline{u'^+_\phi u'^+_\phi}\frac{U^+_\phi}{r^+}}_{\text{Convective transport}}$$

$$-\underbrace{\overline{u'^+_\phi \frac{\partial p'^+}{\partial r^+}} - \overline{u'^+_r \frac{1}{r^+}\frac{\partial p'^+}{\partial \phi}}}_{\text{Velocity pressure gradient}}$$

$$+\underbrace{\frac{1}{\mathrm{Re}_\tau}\left[\frac{1}{r^+}\frac{\partial}{\partial r^+}\left(r^+\frac{\partial \overline{u'^+_r u'^+_\phi}}{\partial r^+}\right) - 4\frac{\overline{u'^+_r u'^+_\phi}}{r^{+^2}}\right]}_{\text{Viscous diffusion}}$$

$$-\underbrace{\frac{2}{\mathrm{Re}_\tau}\left[\overline{\left(\frac{\partial u'^+_r}{\partial r^+}\right)\left(\frac{\partial u'^+_\phi}{\partial r^+}\right)} + \overline{\left(\frac{1}{r^+}\frac{\partial u'^+_r}{\partial \phi} - \frac{u'^+_\phi}{r^+}\right)\left(\frac{1}{r^+}\frac{\partial u'^+_\phi}{\partial \phi} + \frac{u'^+_r}{r^+}\right)} + \overline{\left(\frac{\partial u'^+_r}{\partial z^+}\right)\left(\frac{\partial u'^+_\phi}{\partial z^+}\right)}\right]}_{\text{Dissipation}} \quad (12)$$

Figure 18(a)-(e) shows the Reynolds shear stress $\overline{u'^+_r u'^+_r}$ budget normalized by the friction velocity. The VPG term contributes as the loss at $y^+ < 80$, balances the sum of convection and the production terms. But the contribution becomes inverse at $y^+ > 80$. The gain for the VGP term is most pronounced at $N = 3.0$.

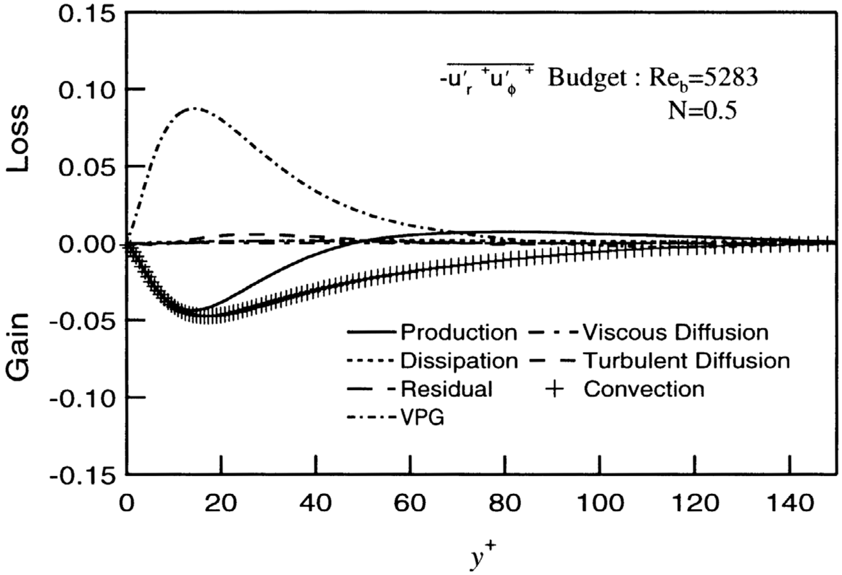

(a)

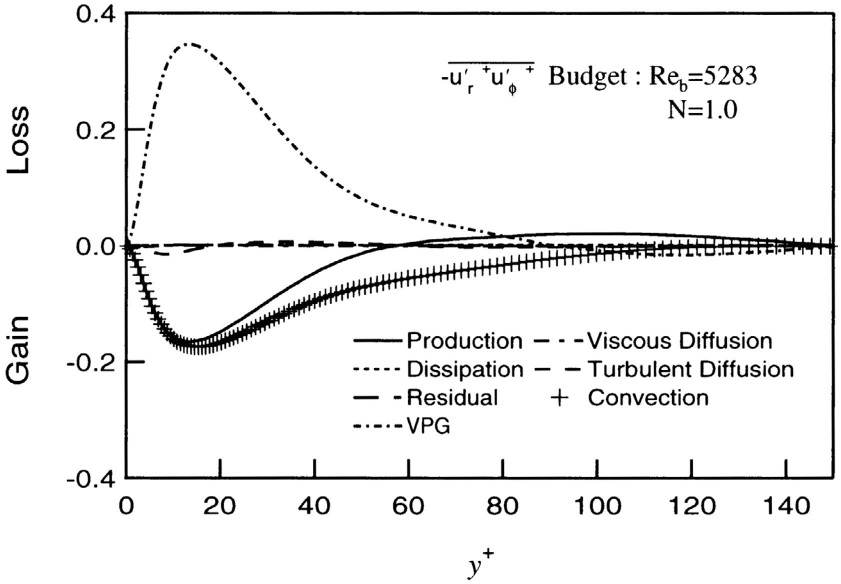

(b)

Figure 18.
The Reynolds shear stress $\overline{u'^+_r u'^+_\phi}$ budget normalized by the friction velocity

(*Continued*)

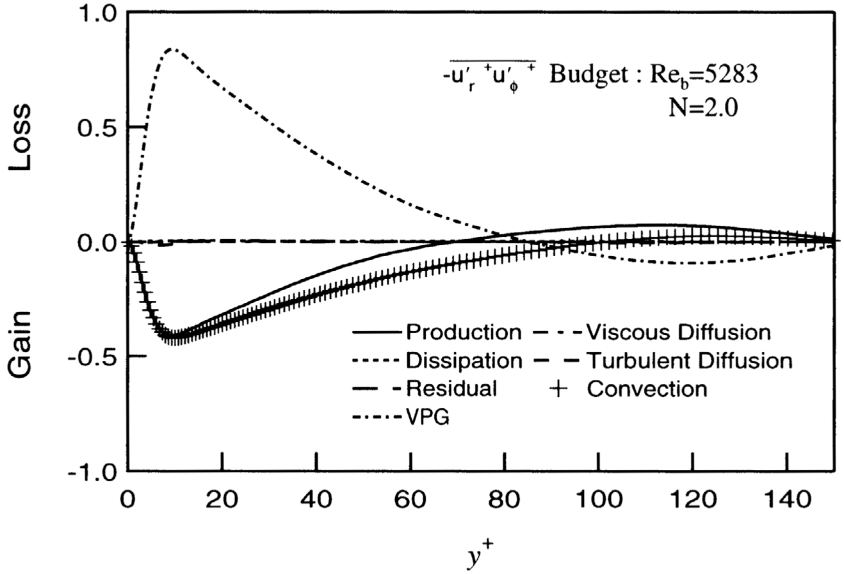
$-\overline{u'^+_r u'^+_\phi}$ Budget : Re_b=5283
N=2.0
Loss
Gain
1.0
0.5
0.0
-0.5
-1.0
0
20
40
60
80
100
120
140
Production
Viscous Diffusion
Dissipation
Turbulent Diffusion
Residual
Convection
VPG
y^+

(c)

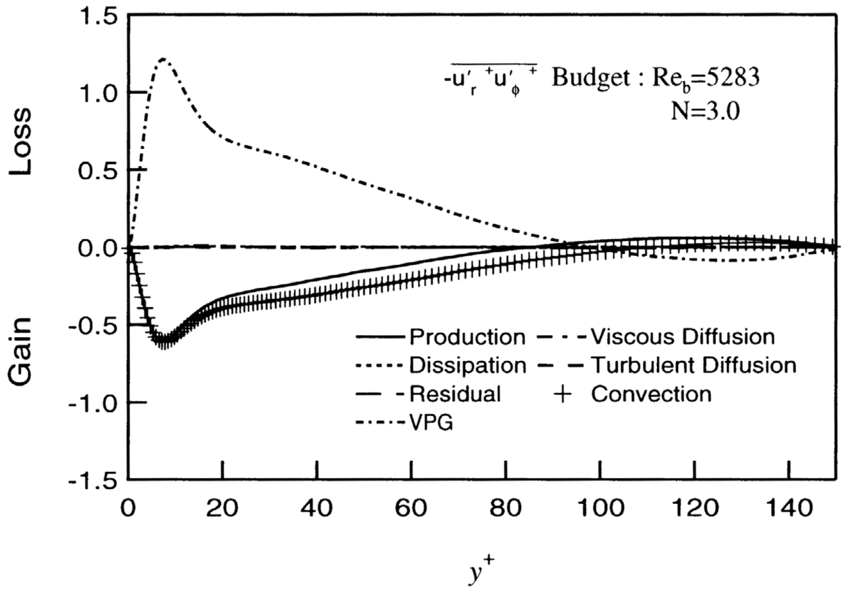
$-\overline{u'^+_r u'^+_\phi}$ Budget : Re_b=5283
N=3.0
Loss
Gain
1.5
1.0
0.5
0.0
-0.5
-1.0
-1.5
0
20
40
60
80
100
120
140
Production
Viscous Diffusion
Dissipation
Turbulent Diffusion
Residual
Convection
VPG
y^+

(d)

Figure 18.

The budget equation for the $\overline{u'^+_r u'^+_r}$ is rewritten as:

$$0 = \underbrace{-\frac{1}{r^+}\frac{\partial r^+ \overline{u'^+_r u'^+_r u'^+_r}}{\partial r^+} + 2\frac{\overline{u'^+_r u'^+_\phi u'^+_\phi}}{r^+}}_{\text{Turbulent diffusion}} \underbrace{+2\overline{u'^+_r u'^+_\phi}\frac{U^+_\phi}{r^+}}_{\text{Production}} \underbrace{+2\overline{u'^+_r u'^+_\phi}\frac{U^+_\phi}{r^+}}_{\text{Convective transport}}$$

$$\underbrace{-2\overline{u'^+_r \frac{\partial p'^+}{\partial r^+}}}_{\text{Velocity pressure gradient}} \underbrace{+\frac{1}{r^+}\frac{\partial}{\partial r^+}\left(r^+\frac{\partial \overline{u'^+_r u'^+_r}}{\partial r^+}\right) - 2\left(\frac{\overline{u'^+_r u'^+_r}}{r^{+^2}} - \frac{\overline{u'^+_\phi u'^+_\phi}}{r^{+^2}}\right)}_{\text{Viscous diffusion}}$$

$$\underbrace{-2\left[\overline{\left(\frac{\partial u'^+_r}{\partial r^+}\right)^2} + \overline{\left(\frac{1}{r^+}\frac{\partial u'^+_r}{\partial \phi} - \frac{u'^+_\phi}{r^+}\right)^2} + \overline{\left(\frac{\partial u'^+_r}{\partial z^+}\right)^2}\right]}_{\text{Dissipation}} \qquad (13)$$

Note that there is direct production term owing to the rotation. Figure 19(a)-(e) shows the Reynolds shear stress $\overline{u'^+_r u'^+_r}$ budget normalized by the friction velocity.

The distribution of the convection and the production terms coincide because of the same expression in equation (13).

These terms are pronounced with the increase of N. At $N = 0.0$, the VPG term contributes as the gain in the whole region.

In consequence of the increase of N, the contribution of the term becomes inverse.

At $N = 3.0$, the term is dominant as the loss, it balances the sum of convection and the production terms. The other terms are negligible compared with the dominant three terms.

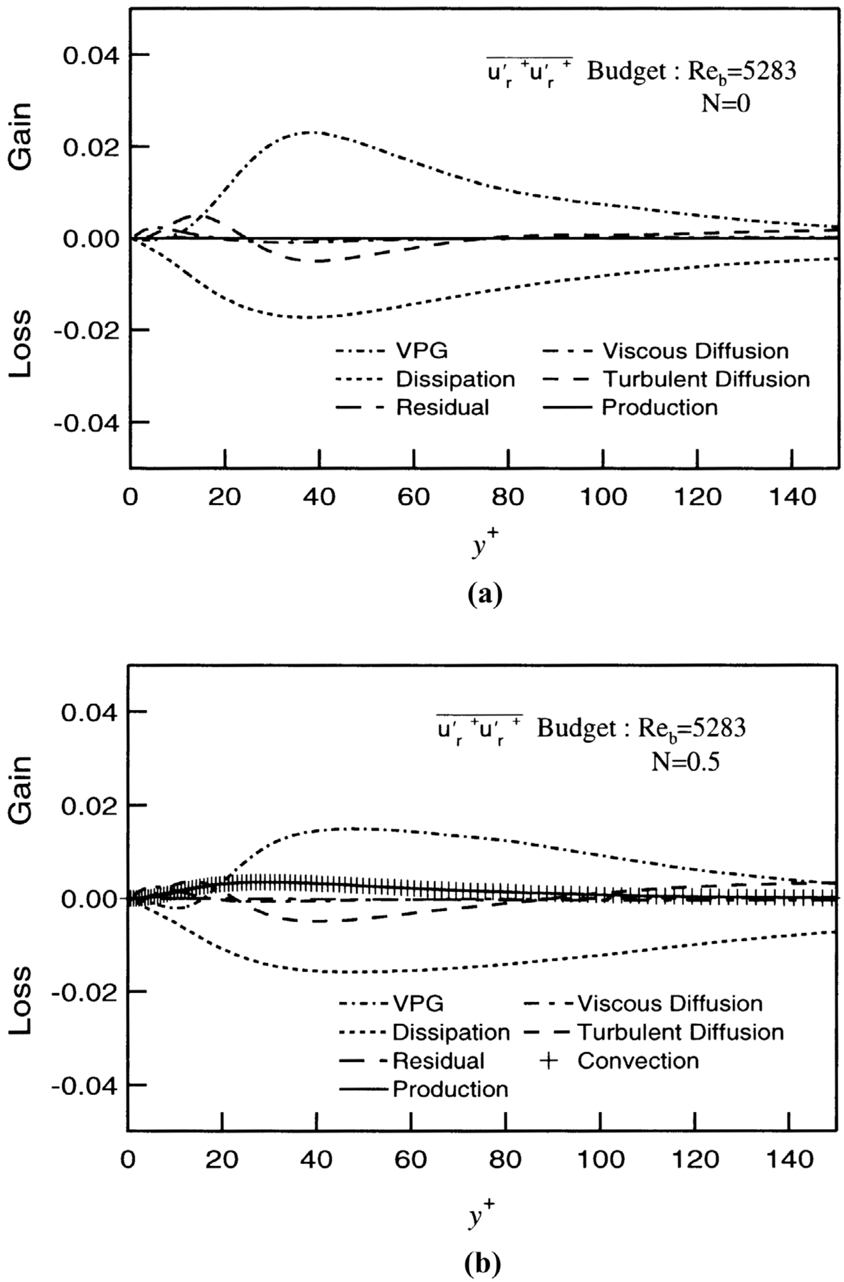

Figure 19.
The Reynolds shear stress $\overline{u'^+_r u'^+_r}$ budget normalized by the friction velocity

(*Continued*)

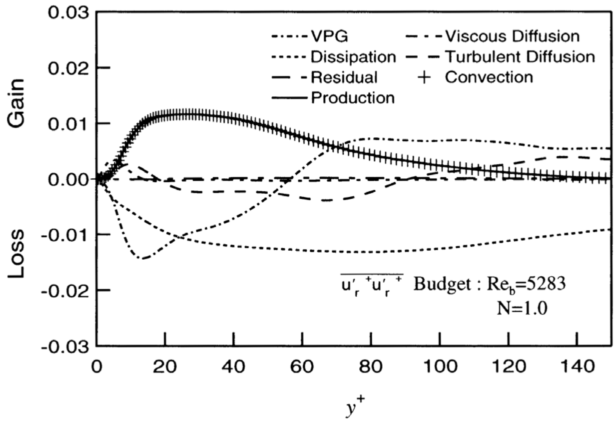

(c)

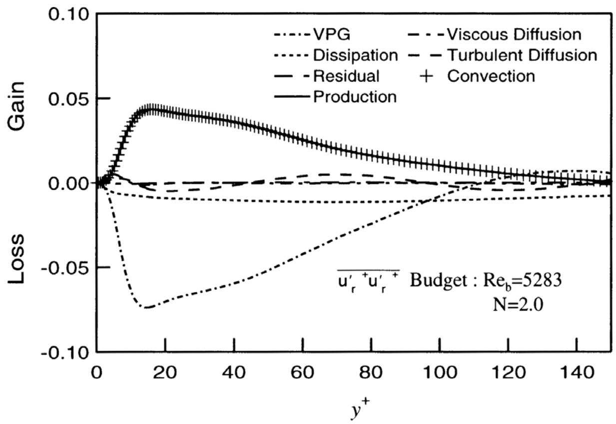

(d)

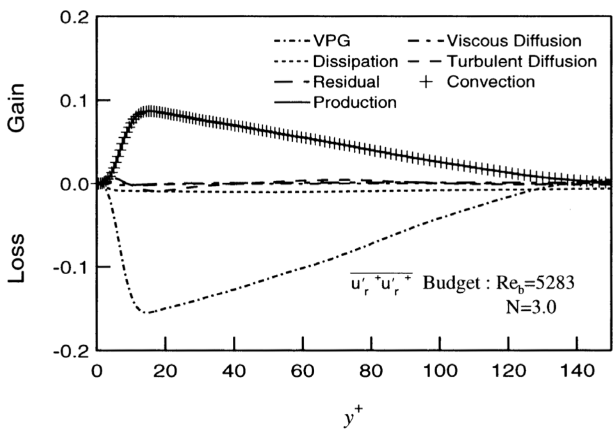

(e)

Figure 19.

The budget equations for the $\overline{u'^{+}_{\phi}u'^{+}_{\phi}}$ is rewritten as:

$$0 = \underbrace{-\frac{1}{r^{+}}\frac{\partial r^{+}\overline{u'^{+}_{r}u'^{+}_{\phi}u'^{+}_{\phi}}}{\partial r^{+}} - 2\frac{\overline{u'^{+}_{r}u'^{+}_{\phi}u'^{+}_{\phi}}}{r^{+}}}_{\text{Turbulent diffusion}} \underbrace{-2\overline{u'^{+}_{r}u'^{+}_{\phi}}\frac{\partial U^{+}_{\phi}}{\partial r^{+}}}_{\text{Production}}$$

$$\underbrace{-2\overline{u'^{+}_{\mathrm{r}}u'^{+}_{\prime}}\frac{U^{+}_{\phi}}{r^{+}}}_{\text{Convective transport}} \underbrace{-\frac{2}{r}\overline{p'^{+}\frac{\partial u'^{+}_{\phi}}{\partial \phi}}}_{\text{Pressure strain}}$$

$$\underbrace{+\frac{1}{r^{+}}\frac{\partial}{\partial r^{+}}\left(r^{+}\frac{\partial \overline{u'^{+}_{\phi}u'^{+}_{\phi}}}{\partial r^{+}}\right) - 2\left(\frac{\overline{u'^{+}_{r}u'^{+}_{r}}}{r^{+2}} - \frac{\overline{u'^{+}_{\phi}u'^{+}_{\phi}}}{r^{+2}}\right)}_{\text{Viscous diffusion}} \tag{14}$$

$$-\underbrace{2\left[\overline{\left(\frac{\partial u'^{+}_{\phi}}{\partial r^{+}}\right)^{2}} + \overline{\left(\frac{1}{r^{+}}\frac{\partial u'^{+}_{\phi}}{\partial \phi} + \frac{u'^{+}_{r}}{r^{+}}\right)^{2}} + \overline{\left(\frac{\partial u'^{+}_{\phi}}{\partial z^{+}}\right)^{2}}\right]}_{\text{Dissipation}}$$

Figure 20(a)-(e) shows the Reynolds shear stress $\overline{u'^{+}_{\phi}u'^{+}_{\phi}}$ budget normalized by the friction velocity.

At the wall, the viscous term balances the dissipation. Although the magnitude of the viscous term and dissipation at the wall is larger than the increase of N, the balance of the two terms is quite similar. But the dissipation, the production and the convection terms drastically change except for near wall region. The convection and the production terms become larger than dissipation and they are balanced with the pressure strain term.

The budget equation of the turbulent heat fluxes for the $u'^{+}_{z}\theta'^{+}$ is rewritten as:

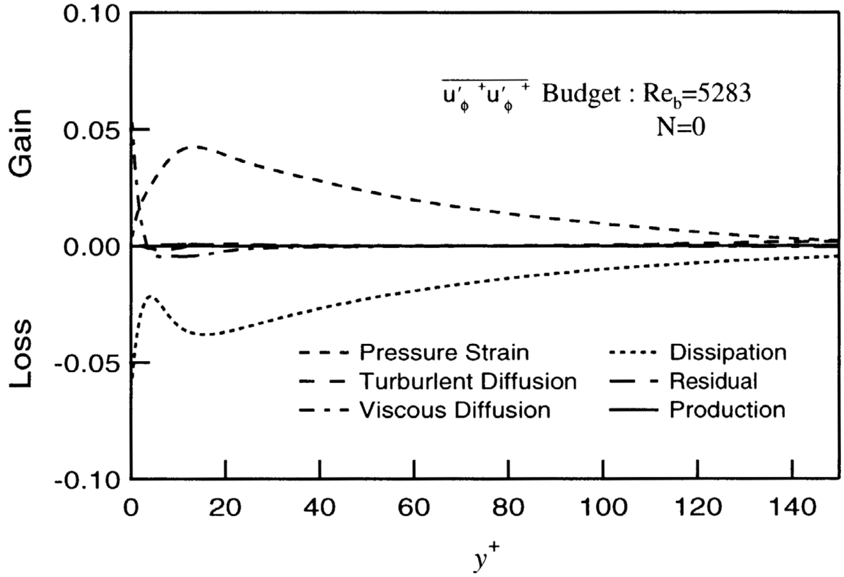

(a)

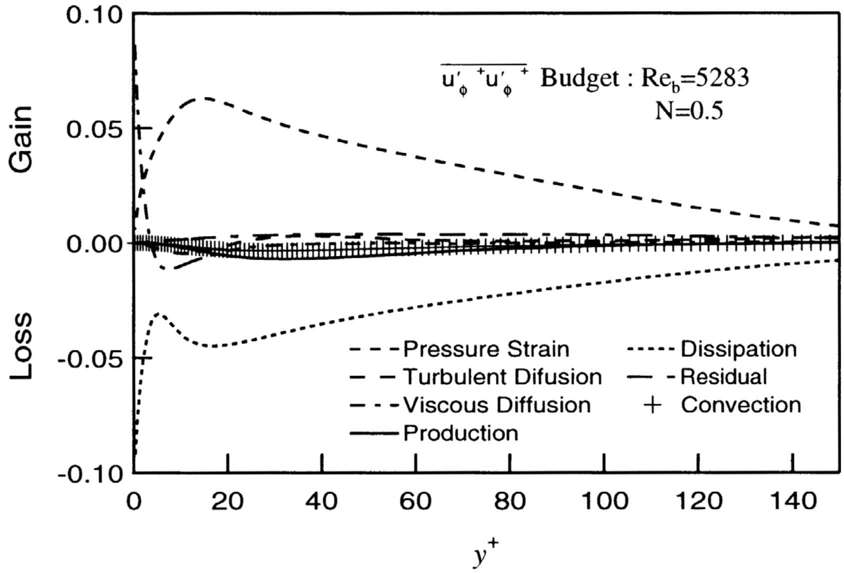

(b)

(*Continued*)

Figure 20.
The Reynolds shear stress $\overline{u'^+_\phi u'^+_\phi}$ budget normalized by the friction velocity

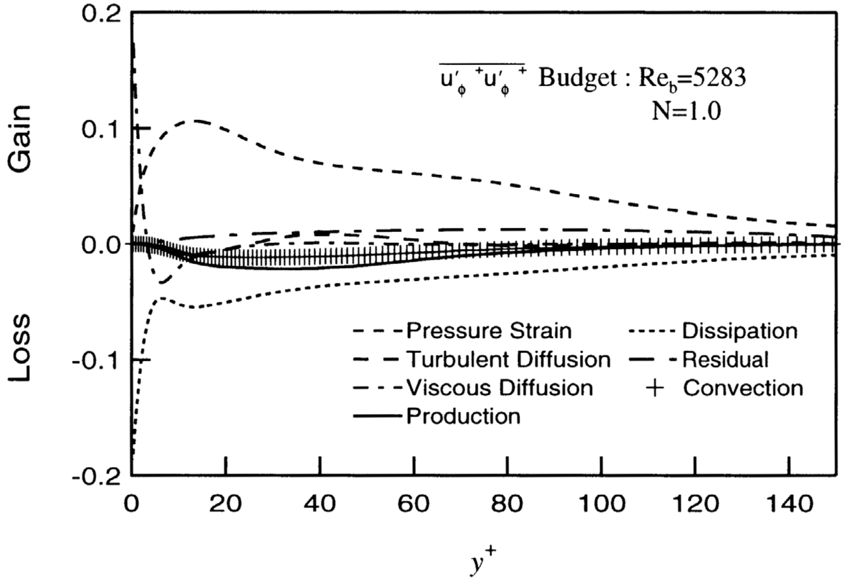

(c)

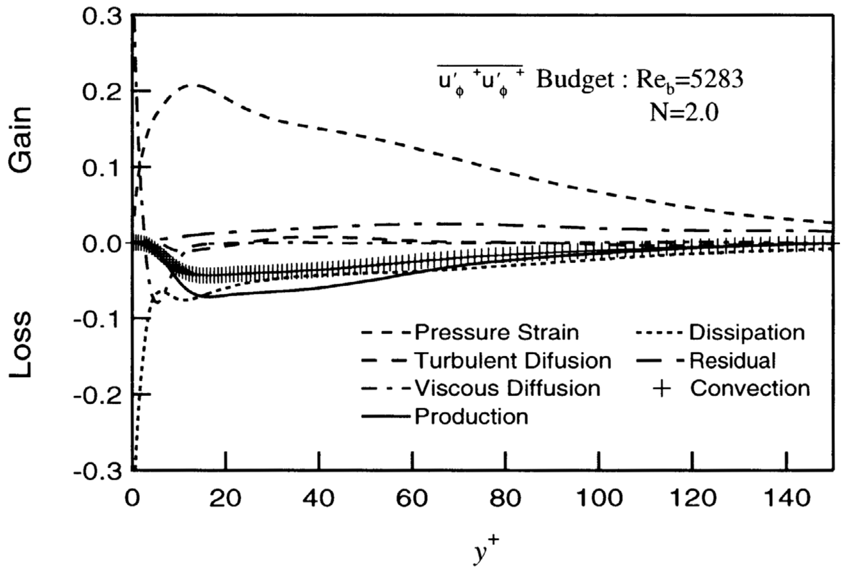

(d)

Figure 20.

(*Continued*)

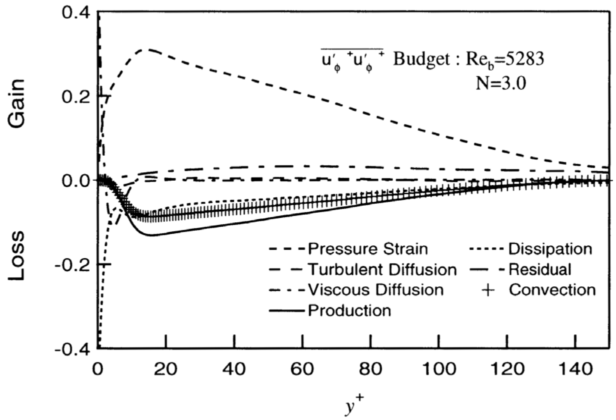

(e)

Figure 20.

$$0 = \underbrace{-\frac{1}{r^+}\frac{\partial r^+\overline{u'^+_z\theta'^+u^+}}{\partial r^+}}_{\text{Turbulent Diffusion}}$$

$$\underbrace{-\overline{u'^+_z u'^+_r}\frac{\partial\Theta^+}{\partial r^+} - \overline{u'^+_r\theta'^+}\frac{\partial U'^+_z}{\partial r^+} + \overline{u'^+_z u'^+_z}\frac{\partial\langle T\rangle}{\partial z^+}}_{\text{Production}} \quad \underbrace{-\overline{\theta'^+\frac{\partial p'^+}{\partial z^+}}}_{\text{Temp. pres. grad.}}$$

$$\underbrace{+\frac{1}{\Pr}\frac{1}{r^+}\frac{\partial}{\partial r^+}\left(r^+\overline{u'^+_z\frac{\partial\theta'^+}{\partial r^+}}\right) + \frac{1}{r^+}\frac{\partial}{\partial r^+}\left(r^+\overline{\theta'^+\frac{\partial u'^+_z}{\partial r^+}}\right)}_{\text{Viscous Diffusion}} \tag{15}$$

$$\underbrace{-\left(\frac{1}{\Pr}+1\right)\left(\overline{\frac{\partial u'^+_z}{\partial z^+}\frac{\partial\theta'^+}{\partial z^+}} + \overline{\frac{\partial u'^+_z}{\partial r^+}\frac{\partial\theta'^+}{\partial r^+}} + \overline{\frac{1}{r^{+^2}}\frac{\partial u'^+_z}{\partial\phi}\frac{\partial\theta'^+}{\partial\phi}}\right)}_{\text{Dissipation}}$$

Figure 21(a)-(e) show the scalar flux $\overline{u'^+_z\theta'^+}$ budget normalized by the friction velocity. It is noted that the pressure-temperature-gradient correlation is a large loss term at $N = 3.0$ and its magnitude is larger than the dissipation term. The sum of temperature-gradient correlation and the dissipation terms

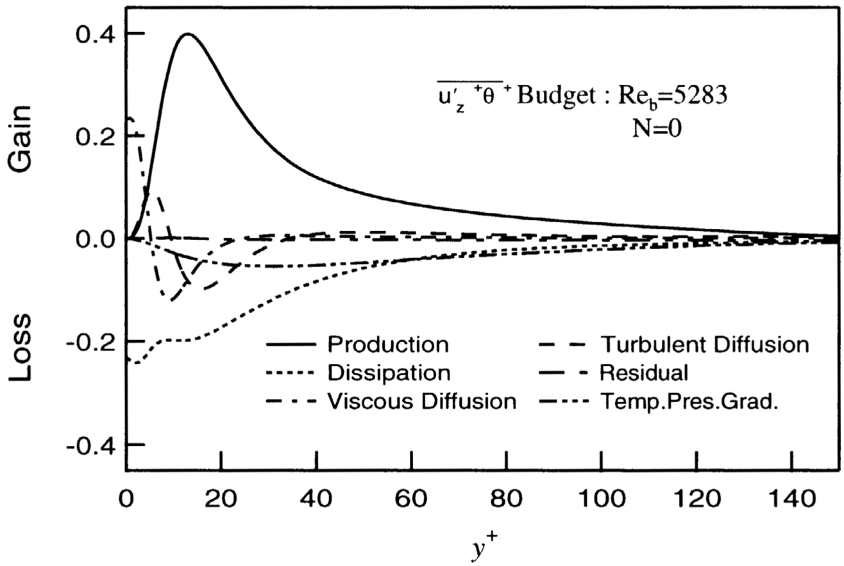

(a)

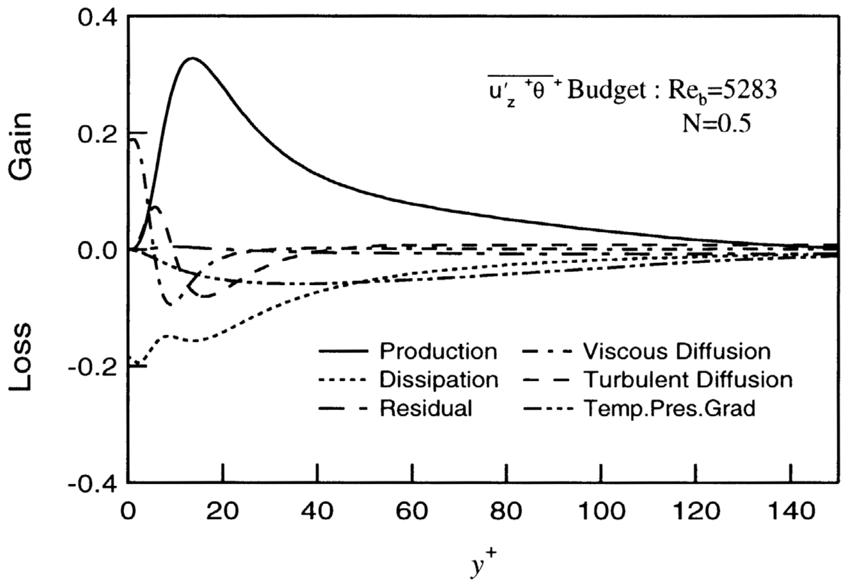

(b)

Figure 21.
The scalar flux $\overline{u'^+_z\theta'^+}$ budget normalized by the friction velocity

(*Continued*)

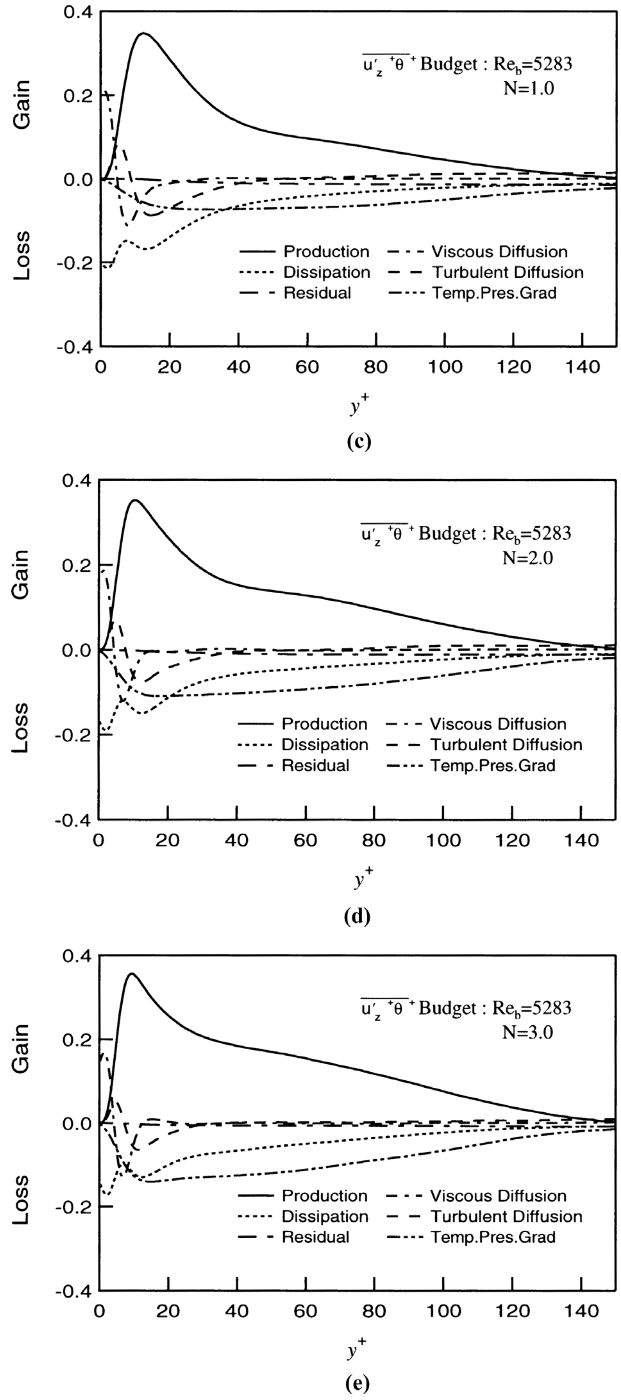
$\overline{u'^+_z\theta^+}$ Budget : Re_b=5283
N=1.0
Gain
Loss
Production
Dissipation
Residual
Viscous Diffusion
Turbulent Diffusion
Temp.Pres.Grad
y^+
(c)
$\overline{u'^+_z\theta^+}$ Budget : Re_b=5283
N=2.0
(d)
$\overline{u'^+_z\theta^+}$ Budget : Re_b=5283
N=3.0
(e)

Figure 21.

are balanced with the production terms. The profiles of each term for $\overline{u'^+_z u'^+_z}$ in Figure 15(a)-(e) are quite similar to the corresponding term for $\overline{u'^+_z \theta'^+}$ in Figure 16(a)-(e). These similarities must be associated with the correlation u'^+_z and θ'^+.

The budget equation of the turbulent heat fluxes for the $\overline{u'^+_r \theta'^+}$ is rewritten as:

$$
\begin{aligned}
0 = & \underbrace{-\frac{1}{r^+}\frac{\partial r^+ \overline{u'^+_r \theta'^+ u'^+_r}}{\partial r^+} + \frac{\overline{\theta'^+ u'^+_\phi u'^+_\phi}}{r^+}}_{\text{Turbulent diffusion}} \underbrace{-\overline{u'^+_r u'^+_r}\frac{\partial \Theta^+}{\partial r^+} + \overline{u'^+_z u'^+_r}\frac{\partial \langle T \rangle^+}{\partial z^+}}_{\text{Production}} \\
& \underbrace{+2\overline{u'^+_\phi \theta'^+}\frac{U^+_\phi}{r^+}}_{\text{Convection}} \underbrace{-\overline{\theta'^+ \frac{\partial p'^+}{\partial r^+}}}_{\text{Temp. pres. grad.}} \\
& \underbrace{+\left\{\frac{1}{r^+}\frac{\partial}{\partial r^+}\left(r^+ \overline{\theta'^+ \frac{\partial u'^+_r}{\partial r^+}}\right) - \overline{\theta'^+ \frac{u'^+_r}{r^{+2}}}\right\} + \frac{1}{\mathrm{Pr}}\frac{1}{r^+}\frac{\partial}{\partial r^+}\left(r^+ \overline{u'^+_r \frac{\partial \theta'^+}{\partial r^+}}\right)}_{\text{Viscous Diffusion}} \\
& \underbrace{-\left(1+\frac{1}{\mathrm{Pr}}\right)\left(\overline{\frac{\partial u'^+_r}{\partial z^+}\frac{\partial \theta'^+}{\partial z^+}} + \overline{\frac{\partial u'^+_r}{\partial r^+}\frac{\partial \theta'^+}{\partial r^+}} + \overline{\frac{1}{r^+}\frac{\partial u'^+_r}{\partial \phi}\frac{1}{r^+}\frac{\partial \theta'^+}{\partial \phi}}\right) - \frac{2}{r^{+2}}\overline{\theta'^+ \frac{\partial u'^+_\phi}{\partial \phi}}}_{\text{Dissipation}}
\end{aligned}
\tag{16}
$$

Figure 22(a)-(e) shows the scalar flux $\overline{u'^+_r \theta'^+}$ budget normalized by the friction velocity. The convection term is larger than the production term except at $N = 0.0$. At $N = 3.0$, temperature-pressure-gradient correlation term is balanced with the sum of the production and the convection terms. The viscous diffusion, dissipation, turbulent diffusion terms are negligibly small.

The budget equation of the turbulent heat fluxes for the $\overline{u'^+_\phi \theta'^+}$ is rewritten as:

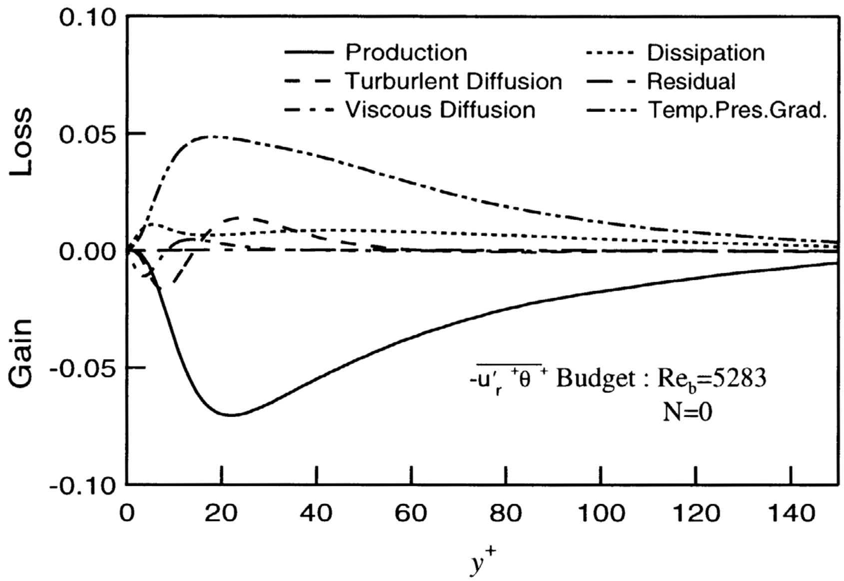

(a)

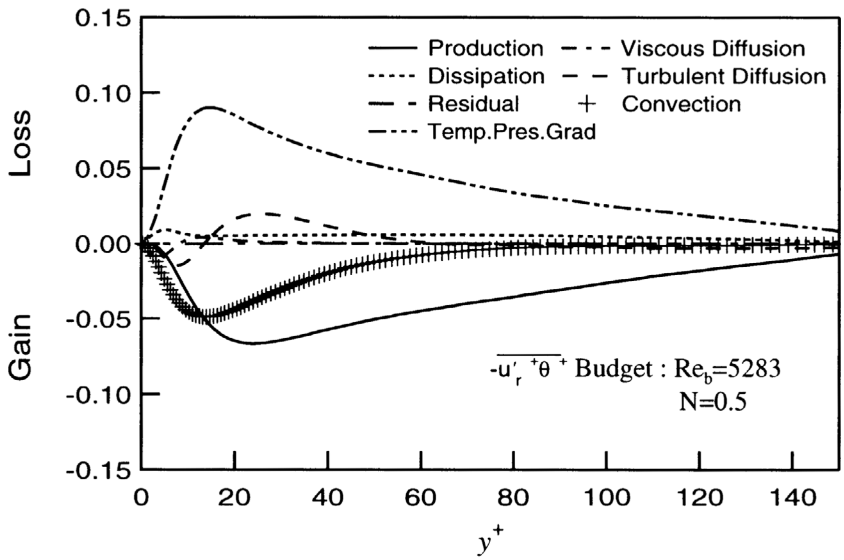

(b)

Figure 22.
The scalar flux $u_r'^{+}\theta'^{+}$ budget normalized by the friction velocity

(*Continued*)

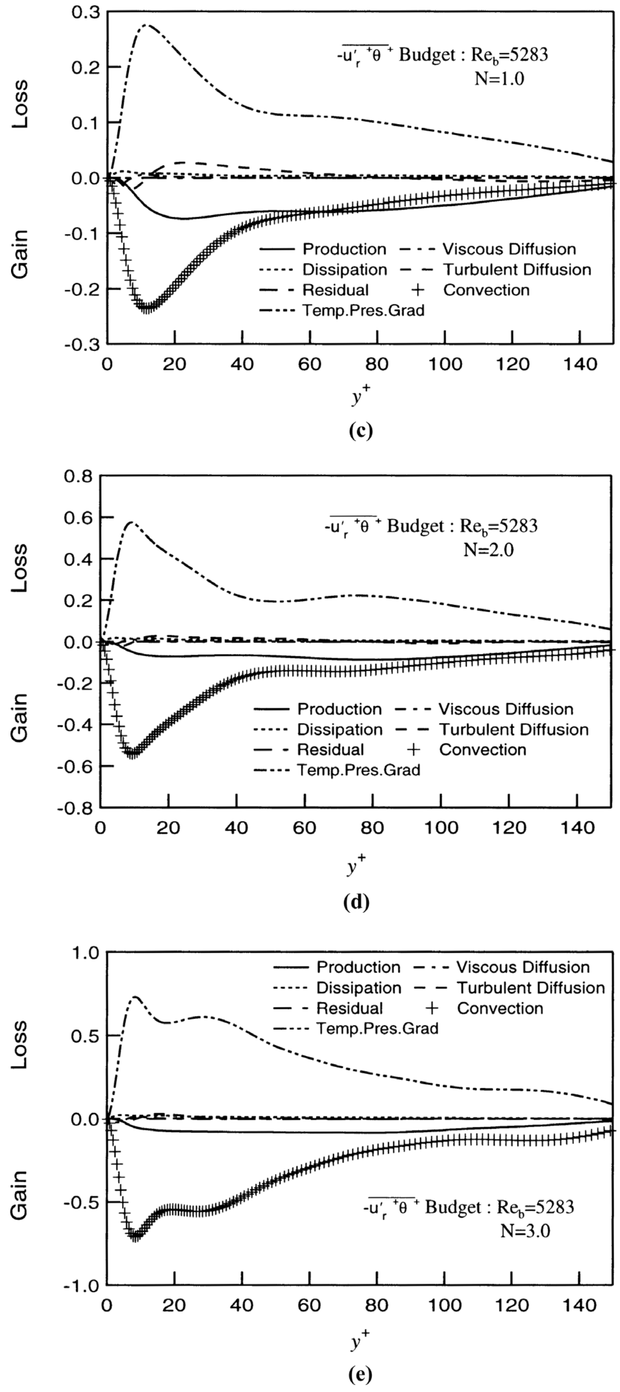
0.3
0.2
0.1
0.0
-0.1
-0.2
-0.3
Loss
Gain
$-\overline{u'_r{}^+\theta^+}$ Budget : Re_b=5283
N=1.0
Production
Viscous Diffusion
Dissipation
Turbulent Diffusion
Residual
Convection
Temp.Pres.Grad
0 20 40 60 80 100 120 140
y^+
(c)
0.8
0.6
0.4
0.2
0.0
-0.2
-0.4
-0.6
-0.8
Loss
Gain
$-\overline{u'_r{}^+\theta^+}$ Budget : Re_b=5283
N=2.0
Production
Viscous Diffusion
Dissipation
Turbulent Diffusion
Residual
Convection
Temp.Pres.Grad
0 20 40 60 80 100 120 140
y^+
(d)
1.0
0.5
0.0
-0.5
-1.0
Loss
Gain
Production
Viscous Diffusion
Dissipation
Turbulent Diffusion
Residual
Convection
Temp.Pres.Grad
$-\overline{u'_r{}^+\theta^+}$ Budget : Re_b=5283
N=3.0
0 20 40 60 80 100 120 140
y^+
(e)

Figure 22.

$$0 = \underbrace{-\frac{1}{r^+}\frac{\partial r^+\overline{u'^+_\phi \theta'^+ u'^+_r}}{\partial r^+} - \frac{\overline{u'^+_\phi \theta'^+ u'^+_r}}{r^+}}_{\text{Turbulent diffusion}}$$

$$\underbrace{-\overline{u'^+_r \theta'^+}\frac{\partial U^+_\phi}{\partial r^+} - \overline{u'^+_r u'^+_\phi}\frac{\partial \Theta^+}{\partial r^+} + \overline{u'^+_z u'^+_\phi}\frac{\partial \langle T\rangle^+}{\partial z^+}}_{\text{Production}} \underbrace{-\overline{u'^+_r \theta'^+}\frac{U^+_\phi}{r^+}}_{\text{Convection}}$$

$$\underbrace{-\frac{1}{r^+}\overline{\theta'^+\frac{\partial p'^+}{\partial \phi}}}_{\text{Temp. pres. grad.}} \qquad (17)$$

$$\underbrace{+\frac{1}{\Pr}\frac{1}{r^+}\frac{\partial}{\partial r^+}\left(r^+\overline{u'^+_\phi\frac{\partial \theta'^+}{\partial r^+}}\right) + \{\frac{1}{r^+}\frac{\partial}{\partial r^+}\left(r^+\overline{\theta'^+\frac{\partial u'^+_\phi}{\partial r^+}}\right) - \overline{\theta'^+\frac{u'^+_\phi}{r^+}}\}}_{\text{Viscous diffusion}}$$

$$\underbrace{-\left(1+\frac{1}{\Pr}\right)\left(\overline{\frac{\partial u'^+_\phi}{\partial z^+}\frac{\partial \theta'^+}{\partial z^+}} + \overline{\frac{\partial u'^+_\phi}{\partial r^+}\frac{\partial \theta'^+}{\partial r^+}} + \frac{1}{r^{+^2}}\overline{\frac{\partial u'^+_\phi}{\partial \phi}\frac{\partial \theta'^+}{\partial \phi}}\right) + \frac{1}{r^{+^2}}\overline{\theta'^+\frac{\partial u'^+_r}{\partial \phi}}}_{\text{Dissipation}}$$

Figure 23(a)-(d) shows the scalar flux $\overline{u'^+_\phi \theta'^+}$ budget normalized by the friction velocity. The whole distribution is similar to those of $u'^+_z u'^+_\phi$ as shown in Figure 17. The temperature-pressure-gradient term is balanced with the sum of the convection and production terms.

To elucidate the energy transfer, the pressure strain correlation is shown in Figure 24(a)-(c). For an ordinary pipe at $N = 0$, the pressure strain term of ϕ_{33} is positive in the whole region as shown in Figure 24(c). The pressure strain term of ϕ_{11} is positive to very in vicinity of the wall and become negative at the other region as shown in Figure 24(a). The pressure strain term of ϕ_{22} is negative near wall region in case of $N = 0$ and 0.5 at $y^+ > 10$ as shown in Figure 24(b). The ordinary redistribution from ϕ_{11} to ϕ_{22} and ϕ_{33} occurs. But at $N = 1.0$, 2.0 and 3.0, the negative region in the pressure strain term of ϕ_{22} disappear in Figure 24(b). This behavior is also shown in $u'^+_r u'^+_r$ budget in Figure 19. Thus, for higher rotating, the redistribution mechanism is completely different compared with the ordinary nonrotating pipe flow.

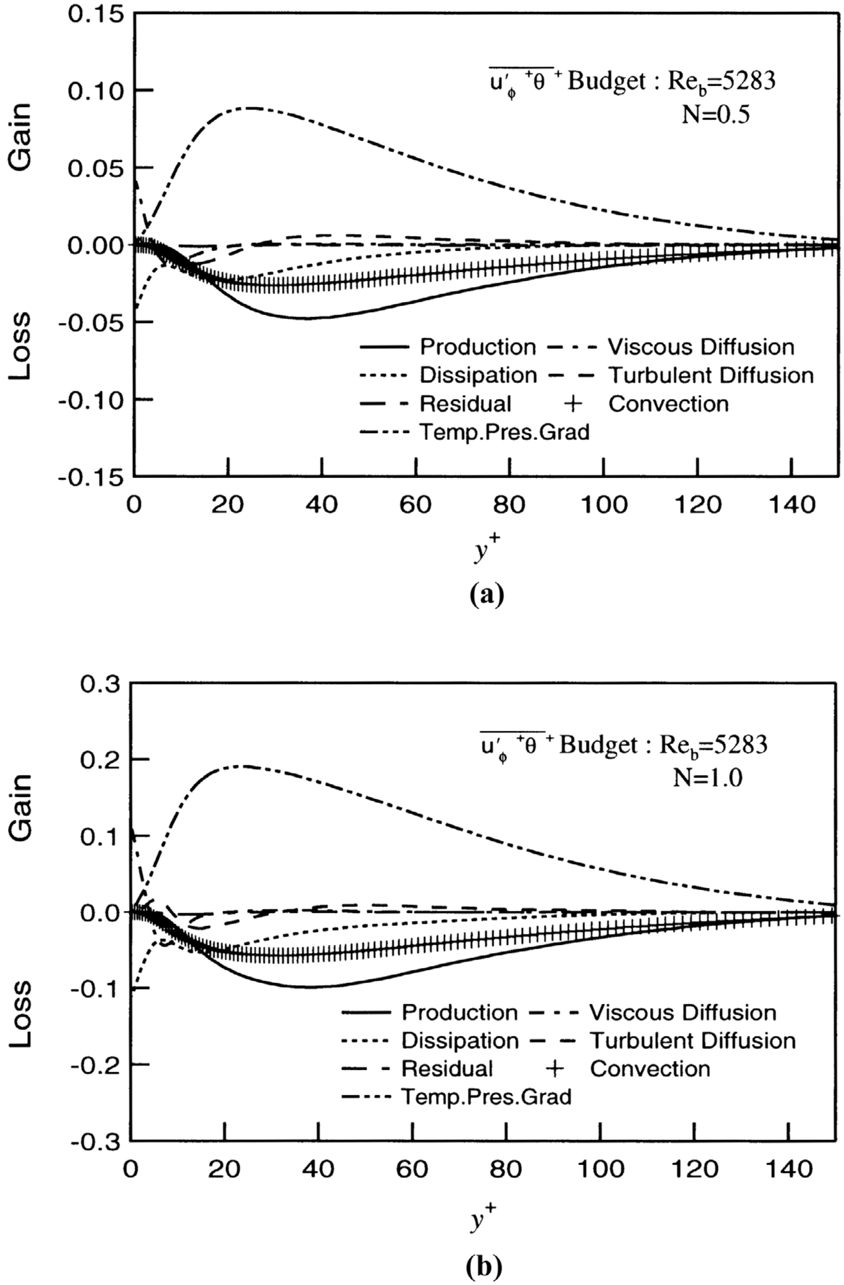

Figure 23.
The scalar flux $\overline{u'^{+}_{\phi}\theta'+}$ budget normalized by the friction velocity

(*Continued*)

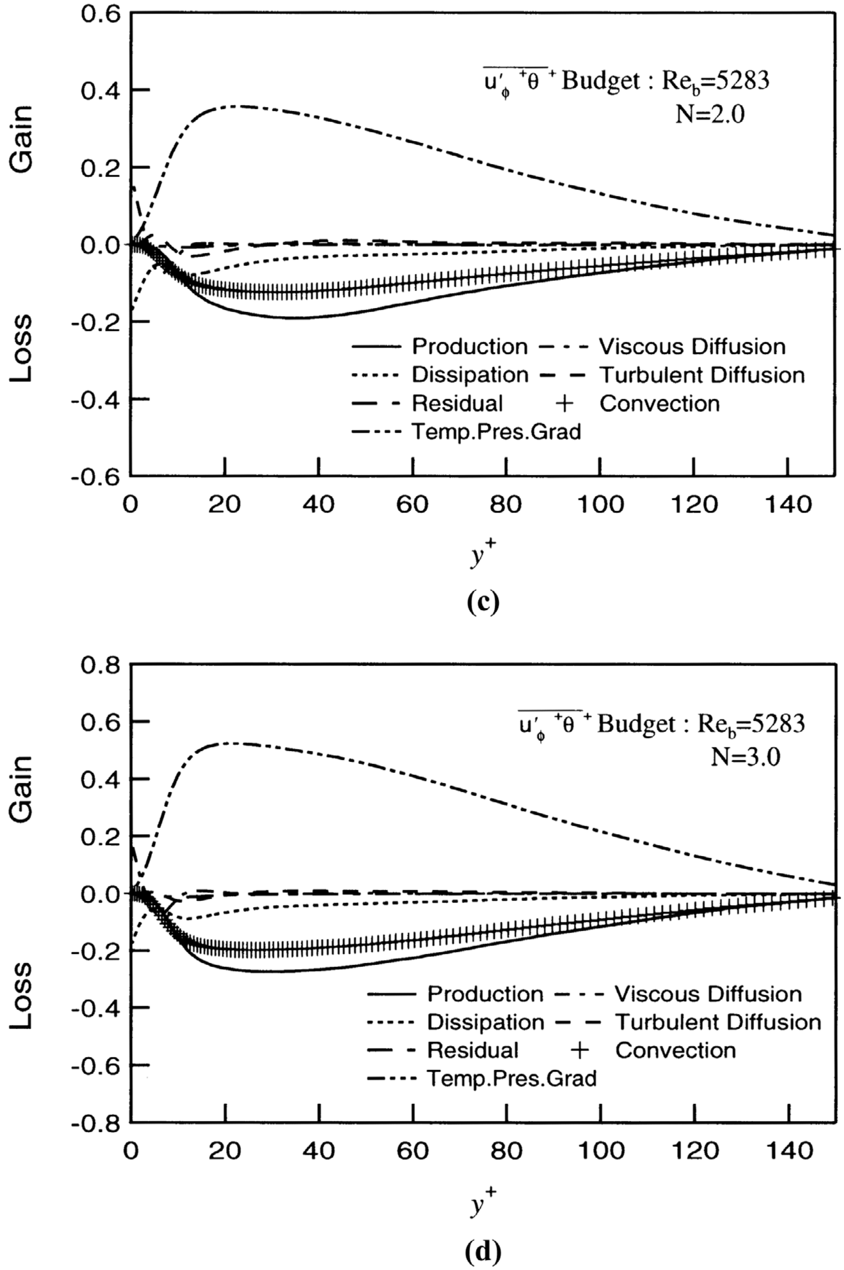
$\overline{u'_\phi{}^+\theta^+}$ Budget : Re_b=5283
N=2.0
Gain
Loss
Production
Viscous Diffusion
Dissipation
Turbulent Diffusion
Residual
Convection
Temp.Pres.Grad
y^+
(c)
$\overline{u'_\phi{}^+\theta^+}$ Budget : Re_b=5283
N=3.0
Gain
Loss
Production
Viscous Diffusion
Dissipation
Turbulent Diffusion
Residual
Convection
Temp.Pres.Grad
y^+
(d)

Figure 23.

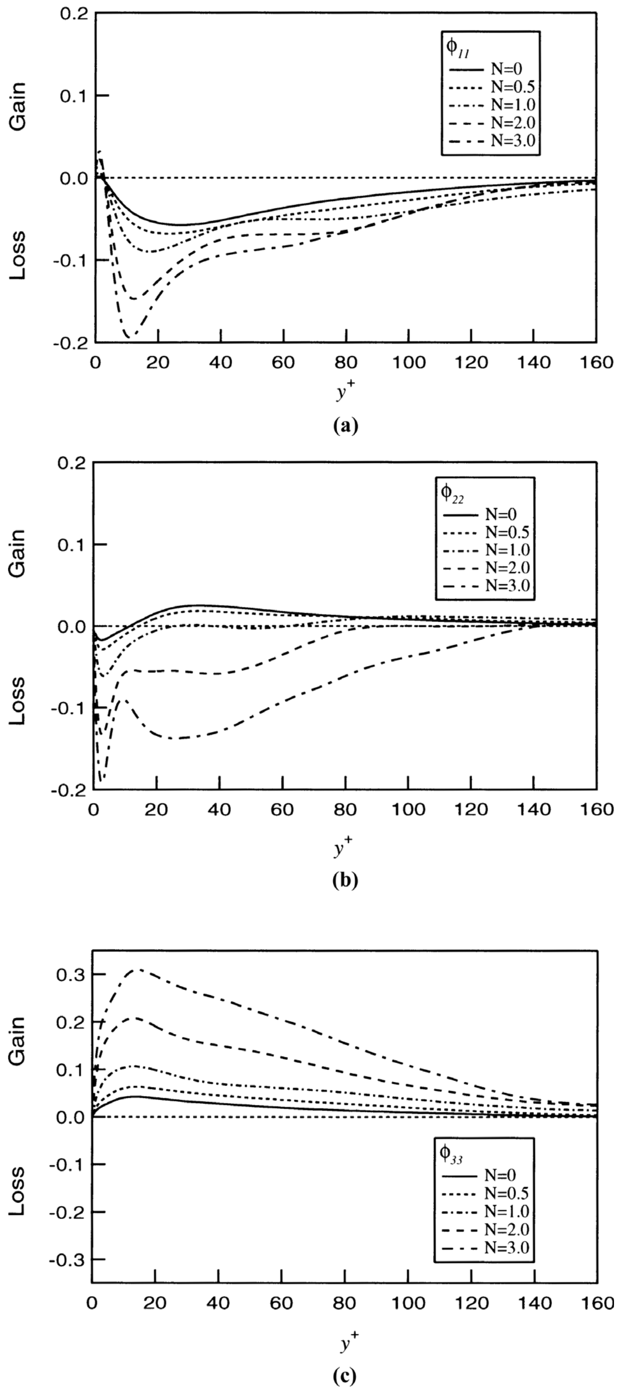

Figure 24.
The pressure strain correlation, (a) ϕ_{11}, (b) ϕ_{22}, (c) ϕ_{33}

The transport process of energy budget in shear stress equation is shown in Figure 25(a). The figure shows the processes of the redistribution, transportation, production, and dissipation. Note that the budget of turbulent kinetic energy, and the diffusion process is not described here. The elliptic symbol shows the production term in Reynolds shear stress equation. Open symbol shows dissipation ε_{ij} in each Reynolds stress equation. The upper region surrounded by chain line defined energy transport mechanism of $N = 0$ and another region surrounded by chain line defined energy transport mechanism of $N \neq 0$. U_ϕ, $\partial U_\phi/\partial r$ is contributed to the production of each stress equation. The pressure strain correlation for normal component ϕ_{11}, ϕ_{22}, ϕ_{33} play a key role of the redistribution process for each stress equations. The transport process of energy budget in scalar flux equation is shown in Figure 25(b). The figure shows the processes of production, and dissipation. Note that the budget of temperature variance $k_\theta = \frac{1}{2}\theta'2$ does not contain the redistribution process for pressure correlation, and the equation must be dissipated by itself. The elliptic symbol shows the production term in scalar flux equation. Open symbol shows dissipation ε_{ij} in each scalar equation. The left region surrounded by chain line defined energy transport mechanism of $N = 0$ and another region surrounded by chain line defined energy transport mechanism of $N \neq 0$. When the rotating causes the production of $u'^+_r\theta'^+$, the stress equation is generated by U_ϕ, $\partial U_\phi/\partial r$ near the wall region. The convection $u'^+_\phi\theta'^+$ associated with mean rotating velocity U_ϕ becomes comparable in magnitude with production term of $N = 3$ considered in Figure 23(d). This energy process contributes production of $u'^+_r\theta'^+$. Thus, the scalar transportation in circumferential connect to the radial direction. When the rotation is high, the terms with U_ϕ, $\partial U_\phi/\partial r$ is dominant compared with other term in $u'^+_r\theta'^+$ and $u'^+_\phi\theta'^+$ flux equations.

Finally, instantaneous flow and temperature fields are visualized to investigate how the near wall structures are affected by the rotating wall. A commercially available 3-D graphics software tool, Application Visualization System (AVS, AVS Inc.), was used for visualization of various turbulence structures. The volume visualized has the half-cut view of the pipe as shown in Figures 26-27. Figure 26(a) for $N = 0.0$, (b) for $N = 2.0$, show the gray and black contour surfaces that represent the low-pressure and low-speed region corresponding to the vortical structure and wall-layer streaks, respectively. At $N = 2.0$, the motion of streaky structure is clockwise, which strongly indicates that this structure is affected by the rotating wall. The vortical structure is observed more frequently and is of larger size, while at $N = 0.0$ they show typical banana-shaped inclined streamwise vortices. Figure 27(a) for $N = 0.0$, (b) for $N = 2.0$ show the gray and black contour surfaces that represent the low-pressure and high-temperature region corresponding to the vortical structure and wall-layer thermal streaks, respectively. Kasagi and Ohtsubo (1993) visualized the location of the thermal streak which are almost same as

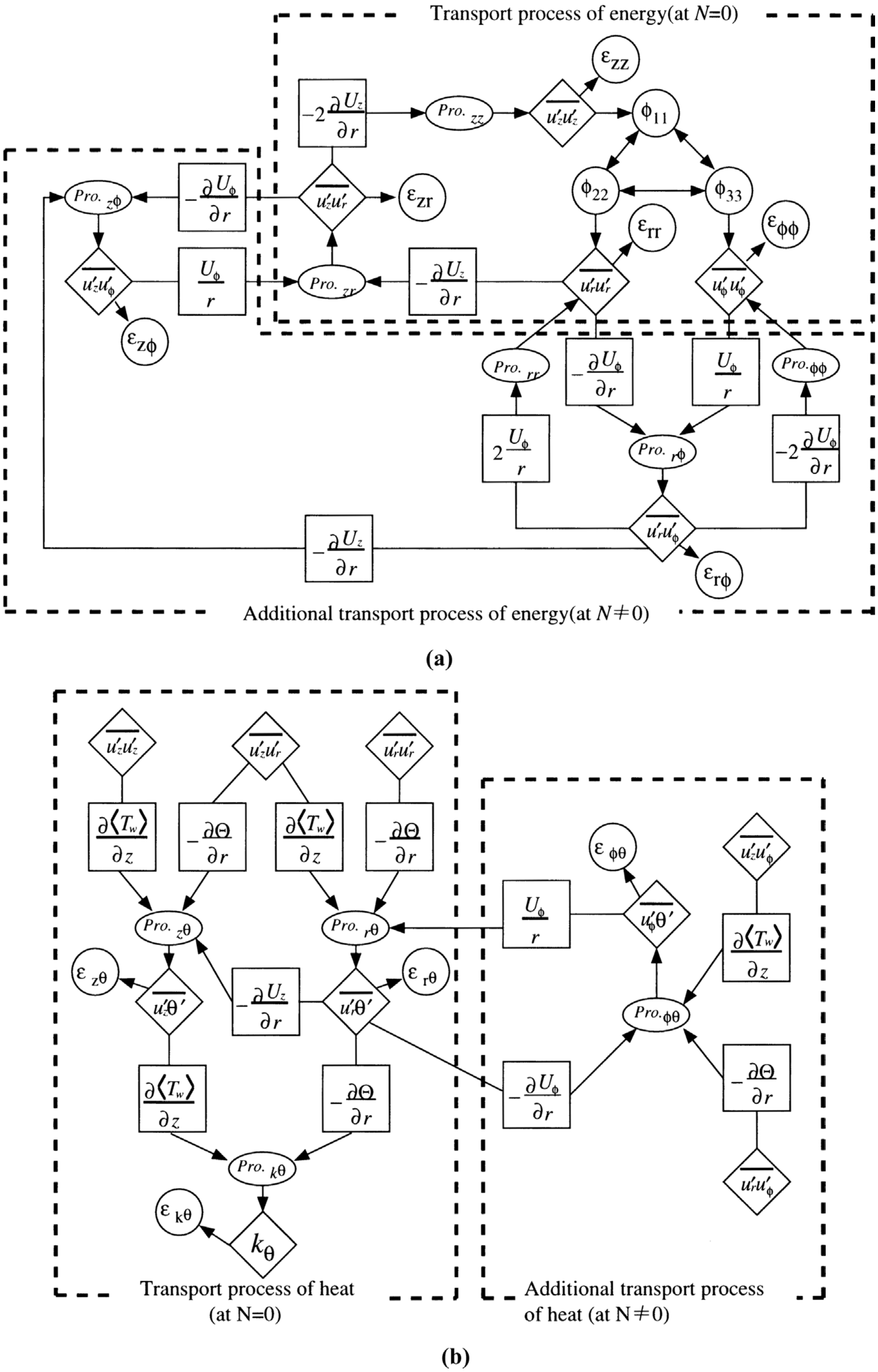

Figure 25.
Energy transport process, (a) Velocity field, (b) Scalar field

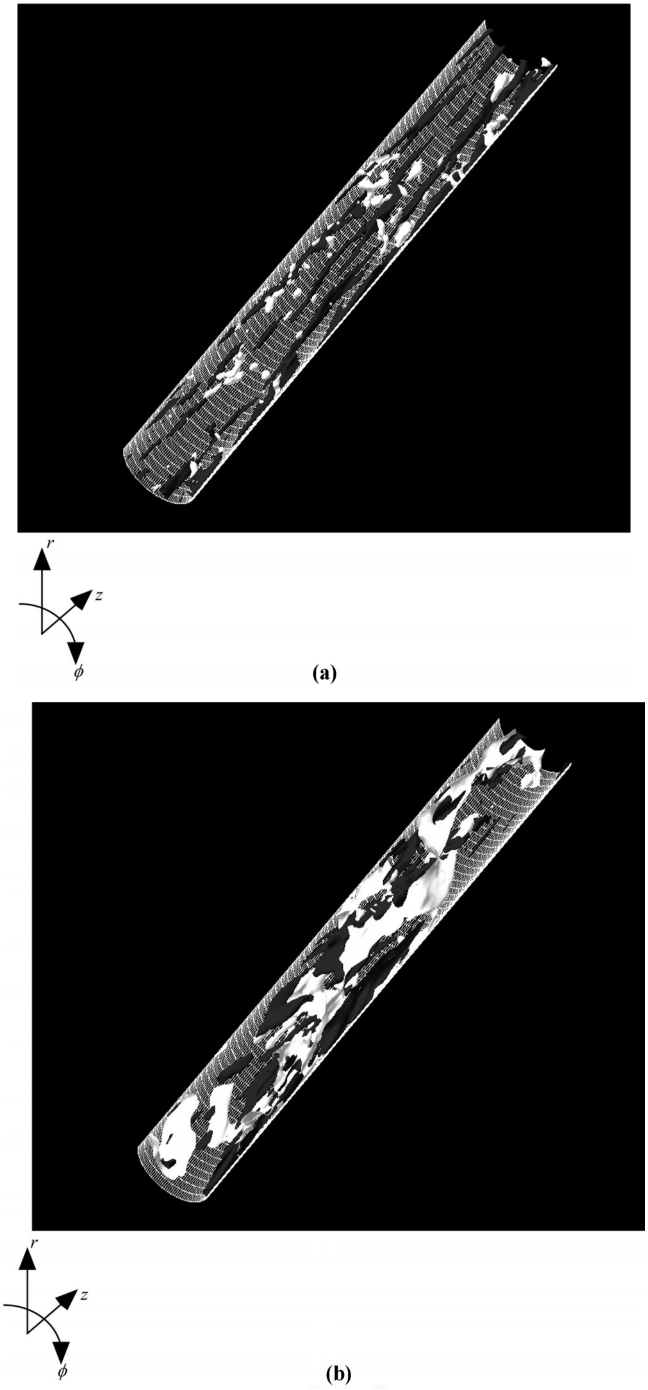

Figure 26.
3-D contour surfaces of low pressure region and low-speed streak, $p'+ < -2$, $u'^{+}_{z} < -3$, $N = 0.0$, $N = 2.0$

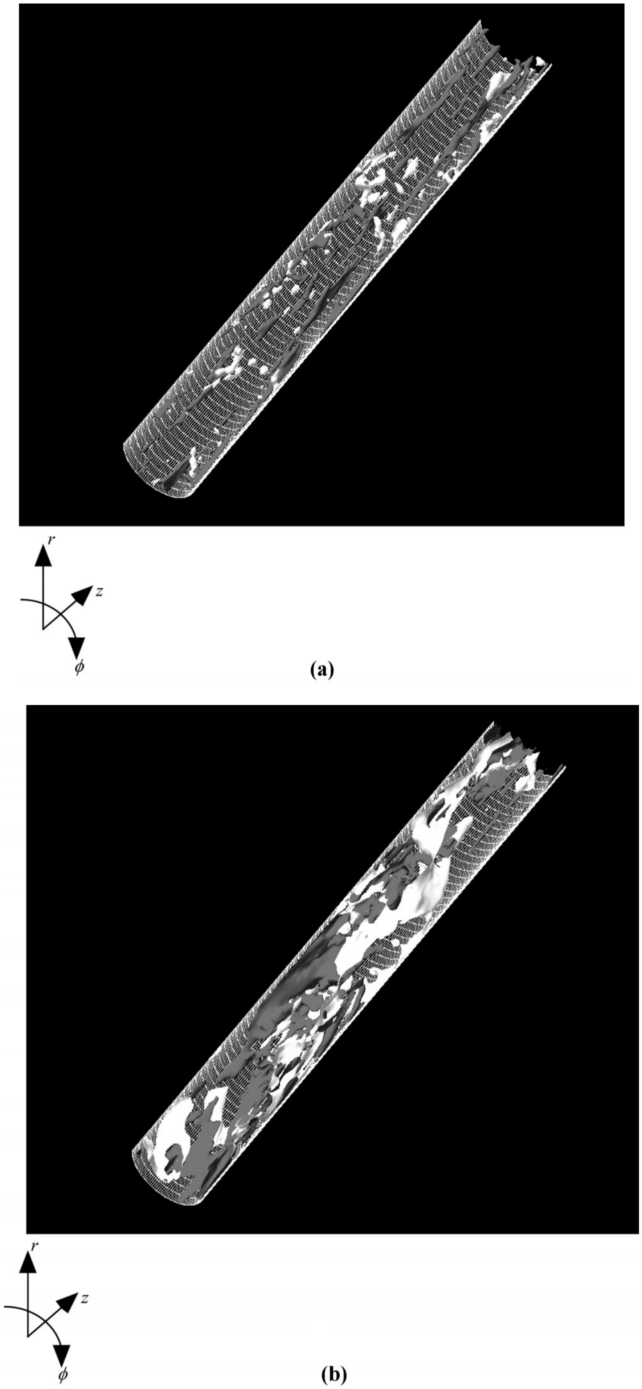

Figure 27.
3-D contour surfaces of low pressure region and thermal streak, $p'+ < -2$, $\theta'+ > 3$, (a) $N = 0.0$, (b) $N = 2.0$

that of low-speed streak in a DNS database of channel flow with $\mathrm{Pr} = 0.71$, also found that the coincidence exists for nonrotating pipe flow as shown in Figures 26(a) and 27(a). For rotating pipe flow, the correlation between thermal streak and low-speed streak is also observed. Thus, the similarity of velocity and temperature in the statistics values also appears in the turbulent structure.

Conclusion

DNS on a turbulent rotating pipe flow with heated wall was carried out for $\mathrm{Re} = 5,283$. The present results for velocity field are in good agreement with the Orlandi and Fatica's DNS data and the Orlandi and Ebstein's DNS data.

In accordance with the distribution of pressure strain correlation, at high *N*, the redistribution mechanism is quite different from that of nonrotating pipe. Especially, in the budget of $u'^{+}_{r}u'^{+}_{r}$, at higher *N*, the VPG term changes the contribution and balances the sum of convection and production term. Then, the other is negligibly small. The scalar flux budget terms obtained are quite similar to the correspondence to the Reynolds shear stress budgets.

References

Cannon, J.N. and Kays, W.M. (1969), "Heat transfer to a fluid flowing inside a pipe rotating about its longitudinal axis", *Transaction ASME J. Heat Transfer*, Vol. 91, p. 135.

Dukowicz, J.K. and Dvinsky, A.S. (1992), "Approximate factorisation as a high order splitting for the implicit incompressible flow equations", *J. Comp. Phys.*, Vol. 102, p. 336.

Eggels, J.G.M. (1994), "Direct and large eddy simulation of turbulent flow in a cylindrical pipe geometry", PhD thesis, Delft University of Technology, The Netherlands.

Eggels, J.G.M., Unger, F., Weiss, M.H., Westerweel, J., Adrian, R.J., Friedrich, R. and Nieuwstadt, F.T.M. (1994), "Fully developed turbulent pipe flow: a comparison between direct numerical simulation and experiment", *J. Fluid Mech.*, Vol. 268, p. 175.

Hirai, S., Takagi, T. and Matsumoto, M. (1988), "Prediction of the laminarization phenomena in an axially rotating pipe flow", *Transaction ASME Journal Fluid Engineering*, Vol. 110, p. 424.

Kasagi, N. and Ohtsubo, Y. (1993), "Direct numerical simulation of low Prandtl number thermal field in a turbulent channel flow", *Turbulent Shear Flow*, Springer, Berlin, Vol. VIII, p. 97.

Kasagi, N., Tomita, Y. and Kuroda, A. (1992), "Direct numerical simulation of passive scalar field in a turbulent channel flow", *Transaction ASME Journal Heat Transfer*, Vol. 114, p. 598.

Kawamura, H. and Mishima, T. (1992), "Numerical prediction of turbulent swirling flow in a rotating pipe by a two-equation model of turbulence (fully developed swirling flow)", *Bulletin JSME*, Vol. 57, p. 1251.

Kawamura, H., Nakamura, S., Satake, S. and Kunugi, T. (1992), "Large eddy simulation of turbulent heat transfer in a concentric annulus", *Thermal Science and Engineering*, Vol. 2, p. 16.

Kikuyama, K., Murakami, M., Nishibori, K. and Maeda, K. (1983), "Flow in an axially rotating pipe (a calculation of flow in the saturated region)", *Bulletin JSME*, Vol. 26, p. 506.

Murakami, M. and Kikuyama, K. (1980), "Turbulent flow in axially rotating pipes", *Trans ASME J. Fluid Engineering*, Vol. 102, p. 97.

Nishibori, K., Kikuyama, K. and Murakami, M. (1987), "Laminarization of turbulent flow in the inlet region of an axially rotating pipe", *JSME International*, Vol. 30, p. 255.

Orlandi, P. (1997), "Helicity fluctuations and turbulent energy production in rotating and non-rotating pipes", *Phys. Fluids*, Vol. 9, p. 2045.

Orlandi, P. and Ebstein (2000), "Turbulent budgets in rotating pipes by DNS", *International Journal of Heat and Fluid Flow*, Vol. 21, p. 499.

Orlandi, P. and Fatica, M. (1997), "Direct simulations of turbulent flow in a pipe rotating about its axis", *J. Fluid Mech.*, Vol. 343, p. 43.

Reich, G. and Beer, H. (1989), "Fluid flow and heat transfer in axially rotating pipe 1. Effect of rotation on turbulent pipe flow", *International Journal Heat Mass Transfer*, Vol. 32, p. 551.

Satake, S. and Kunugi, T. (1998a), "Direct numerical simulation of turbulent pipe flow", *Bulletin JSME*, Vol. 64, p. 65.

Satake, S. and Kunugi, T. (1998b), "Direct numerical simulation of impinging jet flow into parallel disks", *Int. J. of Num. Method Heat and Fluid Flow*, Vol. 8, p. 768.

Satake, S. and Kunugi, T. (1999), "Direct numerical simulation of turbulent heat transfer in an axially rotating pipe flow", *Proc. of 5th ASME/JSME Joint Thermal Engineering Conference*, San Diego, CA, AJTE99-6448.

Spalart, P.R., Moser, R.D. and Rogers, M. (1991), "Spectral methods for the Navier-Stokes equations with one infinite and two periodic directions", *J. Comp. Phys.*, Vol. 96, p. 297.

Verzicco, R. and Orlandi, P. (1996), "A finite-difference scheme for three-dimensional incompressible flows in cylindrical coordinate", *J. Comp. Phys.*, Vol. 123, p. 402.